Article

Current Biology

Comprehensive Chromosome End Remodeling during Programmed DNA Elimination

Graphical Abstract

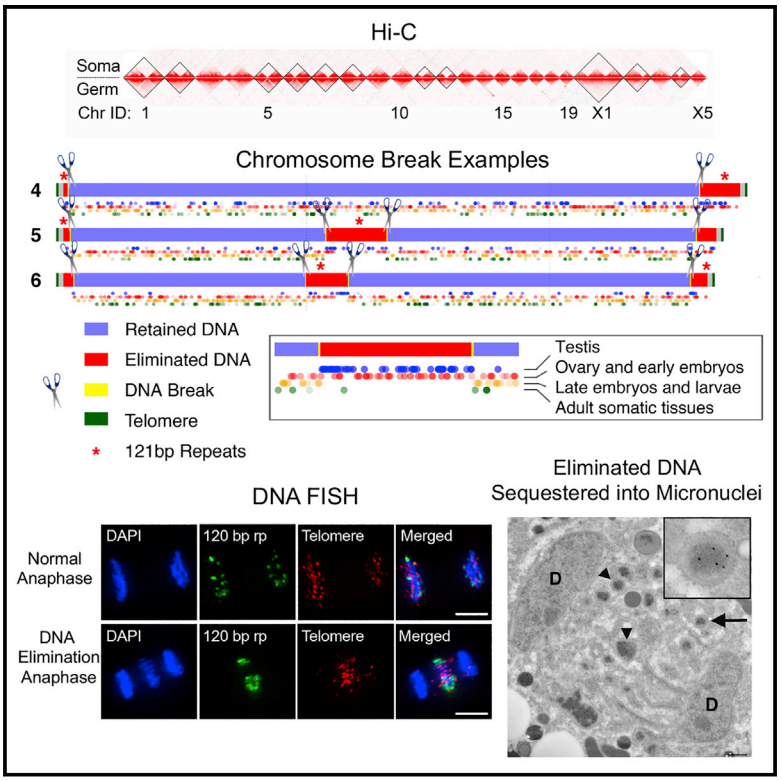

Authors

Jianbin Wang, Giovana M.B. Veronezi, Yuanyuan Kang, Maxim Zagoskin, Eileen T. O'Toole, Richard E. Davis

Correspondence

jianbin.wang@utk.edu (J.W.), richard.davis@cuanschutz.edu (R.E.D.)

In Brief

Comprehensive genome analysis of DNA elimination in the nematode *Ascaris* by Wang et al. provides a chromosome view of DNA elimination demonstrating all chromosome ends undergo subtelomeric DNA breaks, loss of distal sequences, and *de novo* telomere healing. The eliminated DNA is incorporated into micronuclei that become cytoplasmic autophagosomes.

Highlights

- Genome analysis enables a comprehensive chromosome view of nematode DNA elimination
- All chromosome ends undergo subtelomeric DNA breaks and *de novo* telomere addition
- All chromosome regions eliminated contain germline expressed genes
- Eliminated DNA is sequestered into micronuclei and then cytoplasmic autophagosomes

Wang et al., 2020, Current Biology *30*, 3397–3413
September 7, 2020
https://doi.org/10.1016/j.cub.2020.06.058

CellPress

Current Biology

CellPress

Article

Comprehensive Chromosome End Remodeling during Programmed DNA Elimination

Jianbin Wang,[1,2,3,*] Giovana M.B. Veronezi,[1] Yuanyuan Kang,[1,5] Maxim Zagoskin,[1] Eileen T. O'Toole,[4] and Richard E. Davis[1,2,6,*]

[1]Department of Biochemistry and Molecular Genetics, University of Colorado School of Medicine, Aurora, CO 80045, USA
[2]RNA Bioscience Initiative, University of Colorado School of Medicine, Aurora, CO 80045, USA
[3]Department of Biochemistry and Cellular and Molecular Biology, University of Tennessee, Knoxville, TN 37996, USA
[4]Molecular, Cellular and Developmental Biology, University of Colorado at Boulder, Boulder, CO 80309, USA
[5]Present address: Wellman Center for Photomedicine, Massachusetts General Hospital, Harvard Medical School, Boston, MA 02114, USA
[6]Lead Contact
*Correspondence: jianbin.wang@utk.edu (J.W.), richard.davis@cuanschutz.edu (R.E.D.)
https://doi.org/10.1016/j.cub.2020.06.058

SUMMARY

Germline and somatic genomes are in general the same in a multicellular organism. However, programmed DNA elimination leads to a reduced somatic genome compared to germline cells. Previous work on the parasitic nematode *Ascaris* demonstrated that programmed DNA elimination encompasses high-fidelity chromosomal breaks and loss of specific genome sequences including a major tandem repeat of 120 bp and ~1,000 germline-expressed genes. However, the precise chromosomal locations of these repeats, breaks regions, and eliminated genes remained unknown. We used PacBio long-read sequencing and chromosome conformation capture (Hi-C) to obtain fully assembled chromosomes of *Ascaris* germline and somatic genomes, enabling a complete chromosomal view of DNA elimination. We found that all 24 germline chromosomes undergo comprehensive chromosome end remodeling with DNA breaks in their subtelomeric regions and loss of distal sequences including the telomeres at both chromosome ends. All new *Ascaris* somatic chromosome ends are recapped by *de novo* telomere healing. We provide an ultrastructural analysis of *Ascaris* DNA elimination and show that eliminated DNA is incorporated into double membrane-bound structures, similar to micronuclei, during telophase of a DNA elimination mitosis. These micronuclei undergo dynamic changes including loss of active histone marks and localize to the cytoplasm following daughter nuclei formation and cytokinesis where they form autophagosomes. Comparative analysis of nematode chromosomes suggests that chromosome fusions occurred, forming *Ascaris* sex chromosomes that become independent chromosomes following DNA elimination breaks in somatic cells. These studies provide the first chromosomal view and define novel features and functions of metazoan programmed DNA elimination.

INTRODUCTION

Genomes in the diverse cells of a metazoan are typically the same. A variety of mechanisms have evolved to maintain and ensure this genome constancy. Changes in the genome, particularly rearrangements or significant sequence loss, can be deleterious, leading to disease or inviability. However, programmed DNA elimination is a major exception. It occurs in a breadth of evolutionarily diverse organisms ranging from ciliates to mammals [1]. Metazoan DNA elimination occurs primarily in two major forms. In the first form, chromosome loss, one or many chromosomes are eliminated. This form occurs in a few insects, mites, nematodes (*Strongyloides ratti*), hagfish, frogs, songbirds, and marsupials [1–4], and it is typically associated with sex determination or species that reproduce by hybridogenesis [1, 5, 6]. In the second form, chromosomes break with retention of some chromosome fragments and the elimination of others. The elimination only occurs in somatic cells and leads to a distinct and reduced somatic cell genome compared to the germline cell genome. This form of DNA elimination occurs in some parasitic nematodes (ascarids), copepods, ratfish, hagfish, and lampreys [2, 3, 7–14]. Programmed DNA rearrangements also occur in ciliates distinguishing the germline from somatic nuclei [15–19]. However, aspects of DNA elimination in metazoa appear mechanistically distinct from that described in ciliates.

Programmed DNA elimination in ascarid parasitic nematodes results in the loss of 13%–90% of the germline DNA in forming the somatic genome [14, 20]. The majority of eliminated DNA are repetitive sequences organized in tandem repeats that differ in the three genera examined [14]. One to two thousand genes are also eliminated, representing 5%–10% of all genes. We have proposed that DNA elimination in nematodes is a mechanism for silencing germline expressed genes [14, 20]. Instead of using epigenetic mechanisms to silence germline genes in somatic cells, these genes are silenced by their elimination from the genome.

Ascarid programmed DNA elimination involves chromosome breaks, *de novo* telomere healing of the breaks, and the selective

retention and loss of chromosome fragments. Previous analysis of the DNA breaks, called chromosomal break regions (CBRs) [21–23], demonstrated they occur with high fidelity within 3–6 kb regions in the chromosomes of 5 independent pre-somatic cells forming different cell lineages [14, 20]. While the CBRs are high fidelity at the chromosome level, the telomere healing occurs randomly within the CBRs. It is currently not known whether this heterogeneity is due to heterogeneity in DNA breaks or telomere healing. Extensive analyses of CBRs did not identify any sequence, structural motifs, histone marks, small RNAs, or other features that define or target these regions as sites for the chromosome DNA breaks [14]. CBRs, however, become more open or chromatin accessible just prior to and during DNA elimination [14]. *Ascaris* has holocentric chromosomes with centromeres/kinetochores extending along the length of the chromosomes in gametogenic germline cells [24–26]. Prior to DNA elimination, regions of chromosomes that will be lost exhibit reduced CENP-A and kinetochores [26]. During a DNA elimination mitosis, chromosome fragments with reduced CENP-A and kinetochores remain at or near the metaphase plate during anaphase, are not segregated into the newly formed daughter nuclei, and then become localized to the cytoplasm following telophase and cytokinesis where the DNA is eventually degraded. Thus, both discrete sites for DNA breaks and chromosomal changes in centromere/kinetochore localization contribute to DNA elimination and define which chromosome fragments will be retained or eliminated.

Our previous work on *Ascaris* DNA elimination identified many CBRs and the eliminated DNA [14]. However, the previous chromosome assemblies were not sufficient to define the ends of the chromosomes or a comprehensive view of the chromosomal location of the DNA breaks (CBRs) and eliminated DNA. Here, we used in-depth PacBio Sequel II long read sequencing and chromosome conformation capture (Hi-C) to generate comprehensive chromosomal assemblies of *Ascaris* germline and somatic chromosomes. The new genome assemblies enabled us to define the subtelomeric/telomeric regions of all the 24 germline chromosomes and identify the chromosomal location of all CBRs (72 total with 32 new CBRs identified) in the 24 chromosomes, the retained and eliminated DNA regions, and the location and organization of repetitive elements and eliminated genes. DNA fluorescence *in situ* hybridization (FISH) and comparative genome analysis of the ends of germline and somatic chromosome assemblies demonstrated that during DNA elimination both ends of all 24 germline chromosomes undergo subtelomeric DNA breaks (48 total DNA breaks), *de novo* telomere healing of the chromosome ends, and the loss of distal chromosome sequences. These data indicate that all *Ascaris* chromosome ends undergo significant remodeling during DNA elimination. Electron microscopy (EM) studies reveal an ultrastructural timeline of DNA elimination where DNA that will be eliminated does not assemble kinetochores or kinetochore microtubules and is incorporated at telophase into double membrane-bound structures that are reminiscent of micronuclei. Once incorporated into micronuclei, eliminated DNA undergoes chromatin changes and forms autophagosomes in the cytoplasm. Our studies provide the most comprehensive genome analysis of DNA elimination in a metazoan, an ultrastructural timeline of DNA elimination, and identify additional novel and key aspects of metazoan DNA elimination.

RESULTS

PacBio and Hi-C Enable Complete Genome Assembly

Our previous studies established a reference genome for the *Ascaris* germline [14]. However, due to the large 120 bp tandem repeat clusters and other complex repeats including the subtelomeric regions, the technologies used (Illumina, PacBio [average 10 kb reads], and optical mapping) were not sufficient to assemble a comprehensive full-chromosome genome. To overcome this, we generated ~360× raw PacBio Sequel II long reads including ~100× coverage for reads with over 40 kb in length (average 52 kb). The over 40 kb PacBio reads were assembled into 763 contigs (N50 = 4.83 Mb) using Canu [27]. We obtained and used Hi-C data to further scaffold and assemble the germline genome into 24 germline chromosomes (N50 = 12.43 Mb) with only 2.3% of the genome in 84 unplaced contigs (STAR Methods). Our somatic Hi-C data and genome assembly indicate that the germline genome is reduced and split by DNA elimination into 36 somatic chromosomes with no apparent genome recombination or rearrangement (Figure 1).

We identified 19 autosomes and 5 sex chromosomes based on the read coverage for the 24 germline chromosomes (Figure 1; Table 1). The 5 sex chromosomes are consistent with previous cytogenetic analyses [28]. We identified 34 genomic loci in 22 chromosomes for the major 120 bp repeat clusters lost during DNA elimination (hereafter called 120 bp clusters) (Table 1; Figure 2). Most of these clusters exceed the length of the PacBio long reads (50–100 Kb). As the total amount of the eliminated 120 bp DNA is around 30 Mb, we estimate that on average each 120 bp cluster is ~900 Kb. PacBio reads of these clusters consist primarily only of 120 bp repeats and its variants. However, other repetitive sequences can be interspersed and/or flank these 120 bp repeats. Most of the 120 bp clusters are in subtelomeric regions (25) of the chromosomes, while 9 are in internal regions of the chromosomes (Table 1; Figure 2). All of the 120 bp repeat is eliminated from somatic cells. We were able to fully assemble 6 (out of 48) subtelomeric-telomeric regions for *Ascaris* germline chromosomes. For the remaining subtelomeric-telomeric chromosome ends, analysis of the PacBio reads suggests that at least 50–100 kb of subtelomeric repetitive sequence precedes the telomeres (Figure 2) and precluded their complete assembly. Germline telomere length is on average >15 kb, with many PacBio reads for the telomeres exceeding 50 kb.

Overall, we have used long PacBio reads and Hi-C to assemble 24 complete *Ascaris* germline chromosomes including the 5 sex chromosomes. Although this genome assembly is not gap free, we have essentially anchored all sequences into the 24 chromosomes, identified the locations for the 34 large 120 bp repeat clusters, and characterized the organization of the 120 bp repeats as well as the subtelomeric repeats. This complete genome assembly provides a significant new resource for an important parasite infecting upward of 800 million people [29, 30] and enables a chromosomal view of programmed DNA elimination.

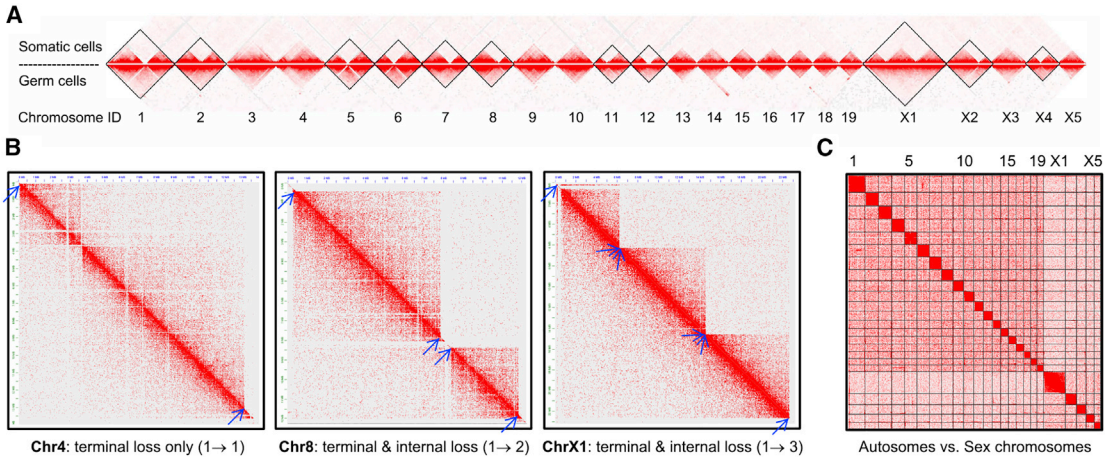

Figure 1. *Ascaris* Chromosome Hi-C Interactions

(A and B) Hi-C interactions in germline and somatic cell genomes (A, overview of all chromosomes; B, selected examples), illustrating the chromosomal changes before and after *Ascaris* DNA elimination.

(A) Hi-C data from germline (testis, bottom) and somatic cells (5-day or 32- to 64-cell embryos, top) were mapped to the 24 assembled *Ascaris* germline chromosomes. The density of the heatmap (Juicebox v1.11.08) indicates the relative contact probability of two loci. The strongest interactions are within chromosomes as illustrated in the 24 germline (bottom) or 36 somatic blocks that correspond to chromosomes (top). Eleven chromosomes (marked in black rhombus boxes) undergo breaks during DNA elimination, leading to an increase in chromosomes. No chromosomal rearrangements were identified in the somatic Hi-C data.

(B) Selected germline chromosomes with the Hi-C interactions are shown (bottom left, germline; top right, somatic). These examples are for germline chromosomes with no internal chromosome changes (Chr4) or increased chromosomes following DNA elimination (Chr8 and ChrX1). Blue arrows point to the CBRs. Note the loss of DNA in the somatic cells at the chromosome ends. See Figure S1 for details of the Hi-C comparisons in all 24 chromosomes.

(C) Hi-C data showing the interactions between *Ascaris* autosomes and sex chromosomes (X1–X5) in the testis. The dataset from (A) was used to illustrate the interchromosomal interactions among *Ascaris* chromosomes.

Gene, Repeat, and Centromere Distribution in *Ascaris* Chromosomes

The general organization of a nematode autosome, primarily from studies from Clade V *C. elegans* [31] and *Pristionchus pacificus* [32, 33], suggests that the middle third of the chromosome is enriched for conserved genes and contains fewer repetitive sequences compared to the chromosome "arms," which have fewer numbers of genes and are repeat rich. The genes in chromosome "arms" are in general not well-conserved or newer genes. In contrast, *Ascaris* autosomes exhibit a relatively uniform distribution of genes with a few gene-poor regions adjacent to subtelomeric regions and the 120 bp repeat clusters, many of which are in internal regions of chromosomes (Figure 2). Repetitive sequences, with the exception of the 120 bp repeat clusters, are relatively uniformly distributed along the chromosomes except for increased repeat levels in subtelomeric regions. Heterochromatic regions (measured by H3K9me2/3 ChIP-seq; data not shown) are in general associated with the repetitive sequences in *Ascaris* chromosomes. *Ascaris* has holocentromeres and the new assembly indicates that the holocentromere/CENP-A is in general distributed along the full length of the chromosomes, consistent with our previous findings [26].

Chromosomal Break Regions for DNA Elimination

We compared germline and somatic genome coverage to identify regions of the genome that were lost following DNA elimination to form the somatic genome [14, 20]. A hallmark of nematode DNA elimination is a chromosome break, the loss of DNA sequences, and the formation of a new chromosome end with a *de novo* telomere in the somatic genome [14, 20–23]. We identified 72 DNA break sites (32 new sites), their chromosomal location, and the formation of new telomeres at the ends of broken chromosomes. All sites of new telomere addition occur heterogeneously within 3–6 kb regions, known as CBRs [14, 20–23]. The CBRs reproducibly occur with high fidelity at specific locations in the chromosomes in all five pre-somatic cells and individuals that undergo DNA elimination [14, 20]. Our sequence analyses of the new CBRs did not identify any specific sequence or structural features (including motifs, hairpins, palindromes, G-quadruplexes, Z-DNA, or repetitive sequences) within or near the CBRs or small RNAs targeting the regions that might specify or recruit machinery to the CBRs as previously described [14, 20–23]. However, as for the previously described CBRs, the newly identified CBRs all become more chromatin accessible (measured by ATAC-seq) just before the DNA elimination mitosis [14] (Figure S2).

DNA Elimination Remodels the Ends of All Germline Chromosomes

DNA FISH using a telomere probe indicated that telomeres on all chromosomes are reduced below detection during a DNA elimination mitosis (Figures 3A–3C). Telomere re-extension on the chromosomes seems to be heterogeneous and take multiple cell cycles to reach signal intensity similar to the germline cell levels (Figures 3D and 3E). Similar observations were made previously by Niedermaier and Moritz [28]. The new genome assembly provided information on the subtelomeric regions of the

Table 1. *Ascaris* Germline and Somatic Chromosomes

Germline Chromosome Name	Germline Assembled Length (Mb)	Terminal CBRs	Internal CBRs	Somatic Chromosome Number	Somatic Chromosome Length (Mb)	PacBio Reads (X)	120 bp Position[a]	120 bp Sites	Eliminated Left End (Kb)	Eliminated Internal (Kb)	Eliminated Right End (Kb)
chr1	18.84	2	2	2	9.86; 7.18	206	MR	2	145	1,254	352
chr2	14.21	2	2	2	7.19; 6.22	219	R	1	218	132	404
chr3	14.13	2	0	1	13.32	215	LR	2	601	0	184
chr4	13.92	2	0	1	12.98	207	LR	2	90	0	829
chr5	13.43	2	2	2	5.25; 6.36	216	LM	2	138	1,248	402
chr6	13.25	2	2	2	4.75; 7.03	207	MR	2	209	872	347
chr7	13.14	2	2	2	7.12; 4.41	213	LMR	3	141	1,020	406
chr8	12.19	2	2	2	7.40; 3.54	209	M	1	392	444	371
chr9	11.53	2	0	1	11.33	200	–	0	104	0	79
chr10	11.05	2	0	1	10.40	211	L	1	298	0	328
chr11	10.27	2	2	2	2.87; 5.98	217	MR	2	287	882	204
chr12	9.83	2	2	2	4.08; 3.90	203	LM	2	198	1,611	3
chr13	8.68	2	0	1	8.23	209	L	1	253	0	178
chr14	8.49	2	0	1	8.31	221	L	1	98	0	60
chr15	8.25	2	0	1	7.62	215	LR	2	333	0	286
chr16	8.14	2	0	1	7.78	190	R	1	168	0	173
chr17	7.35	2	0	1	7.02	199	L	1	114	0	190
chr18	7.08	2	0	1	6.59	219	R	1	96	0	380
chr19	7.08	2	0	1	6.37	210	–	0	104	0	586
chrX1	23.12	2	4	3	6.06; 8.25; 8.05	166	LR	2	122	43 and 49	481
chrX2	12.43[b]	2	2	2	8.65; 3.13	171	M	1	95	478	43
chrX3	9.86	2	0	1	9.40	171	R	1	66	0	372
chrX4	8.97	2	2	2	3.69; 4.51	162	MR	2	24	290	409
chrX5	7.14	2	0	1	6.88	164	L	1	208	0	26
Total	272.37 Mb	48	24	36	251.74 Mb	–	–	34	4.50 Mb	8.32 Mb	7.09 Mb

[a]L, left; M, internal; R, right
[b]N50 = 12.43 Mb (the 9th largest chromosome)

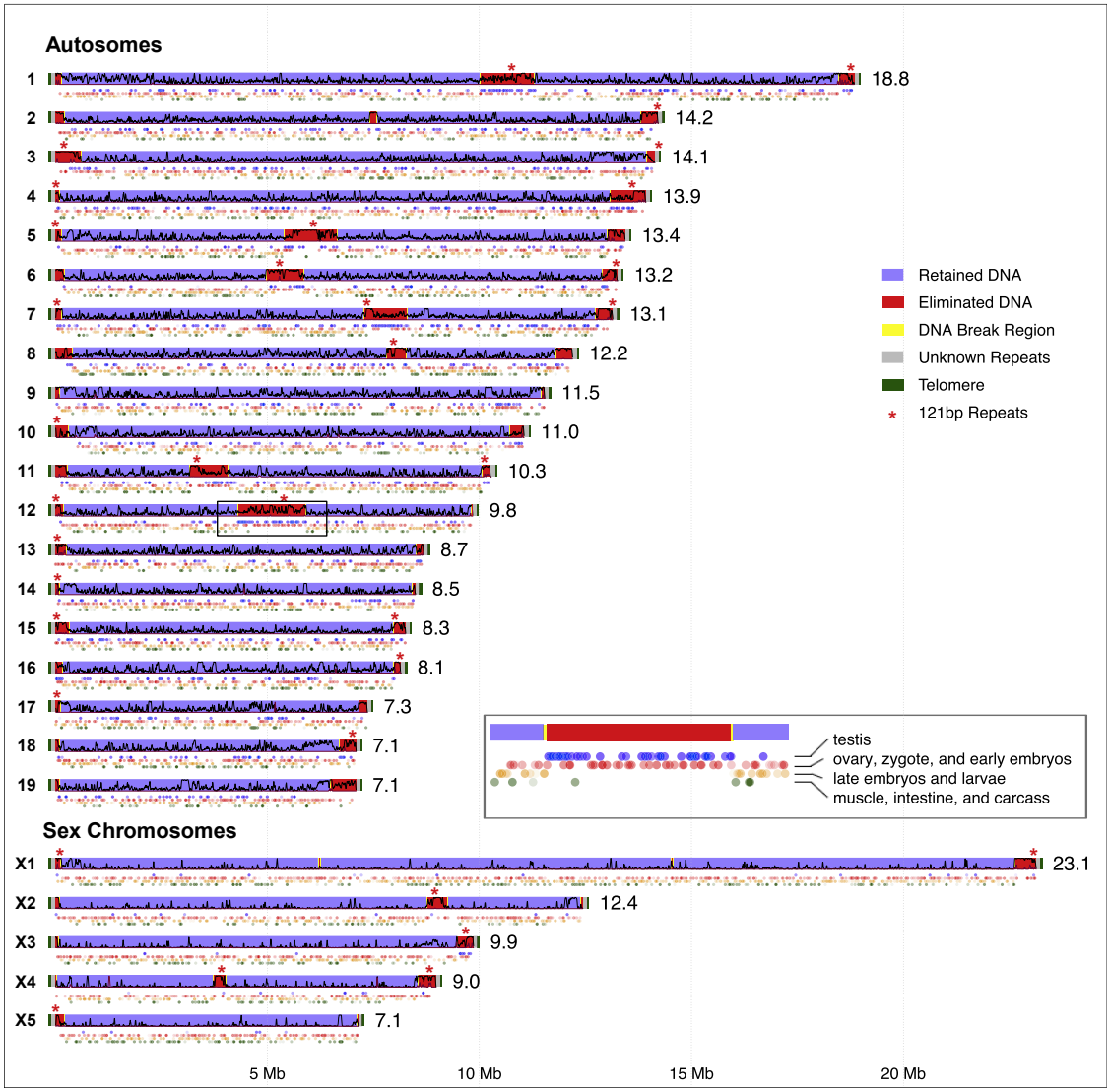

Figure 2. *Ascaris* Chromosomes and Programmed DNA Elimination

Chromosomes are illustrated with the length of the chromosome in Mb on the right. Each dot beneath the chromosomes is a gene with the color and transparency indicating the extent of tissue-specific expression (see the boxed enlarged region from chr12 for legend). Over 70% of all expressed were plotted. The repetitive sequences in % for a 20-kb window size (with a 4-kb sliding window) in *Ascaris* chromosomes are illustrated vertically within the chromosome bars, with simple satellite repeats in red and all other repeats in black across the chromosome. See also Figure S2.

germline chromosomes that were previously not well assembled. Comparison of the germline and somatic chromosome termini strikingly demonstrated that CBRs occurred in all subtelomeric regions at both ends of each chromosome (2 × 24 = 48 terminal CBRs in *Ascaris* genome) (Figure 2; Table 1). Thus, the data indicate that during DNA elimination all germline chromosome ends undergo subtelomeric breaks, with the loss of distal regions including the telomeres. Our somatic sequencing suggests that the new chromosome ends are healed by *de novo* telomere addition.

To confirm that the ends of chromosomes were lost during DNA elimination, we carried out DNA FISH using specific subtelomeric probes on each side of the subtelomeric chromosome breaks. As shown in Figures 3F and 3H, subtelomeric probes corresponding to the eliminated side of a break remain at the metaphase plate during a DNA elimination mitosis and are not undergoing segregation. In contrast, subtelomeric probes corresponding to the retained side of a break are segregated to daughter nuclei. In addition, DNA FISH with probes corresponding to retained and eliminated regions of internal DNA breaks are also consistent with genome data for DNA breaks and sequences lost or retained (Figures 3F and 3G). Consistently, in later stage embryos (8–32+ cells), DNA FISH shows that the eliminated DNA derived from the ends or internal regions of chromosome is absent in somatic nuclei (Figure S3). Overall, our DNA FISH and genome comparisons demonstrate that DNA breaks in subtelomeric regions of chromosomes lead to the loss of all chromosomes

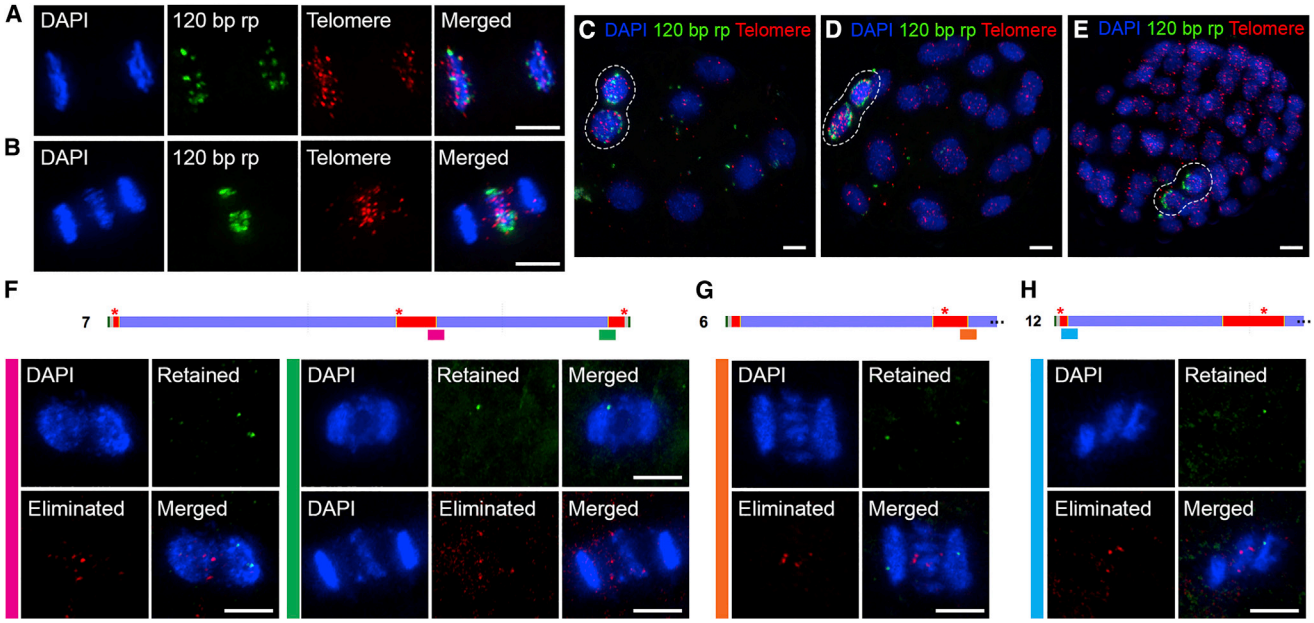

Figure 3. Subtelomeric and Telomeric Loss in DNA Elimination

(A) DNA FISH of a non-DNA elimination anaphase in a 3-cell embryo showing that the telomeric and 120 bp tandem repeat DNA are segregated.

(B) DNA FISH of a DNA elimination anaphase in a 4-cell embryo showing that the telomeric and 120 bp repeat DNA remain at the metaphase plate. DNA remaining at the metaphase plate is eliminated.

(C) DNA FISH shows telomeric and 120 bp repeat DNA are not incorporated into daughter nuclei and become cytoplasmic (8-cell embryo). Note the absence of telomeric signal (and 120 bp repeat) in somatic nuclei that have undergone DNA elimination compared to the two germ cells (dotted circle).

(D and E) DNA FISH shows the dynamics of telomere re-extension in somatic nuclei after DNA elimination.

(D) Post-elimination somatic nuclei in a 24-cell embryo show less telomeric DNA FISH signal with heterogeneous intensities compared to germ cells (dotted circle).

(E) DNA FISH for telomeres in somatic nuclei of a 64+-cell embryo shows comparable signal intensities to the germ cells (dotted circle). Single channel images for (C)–(E) are shown in Figure S3.

(F) DNA FISH on internal and terminal chromosome 7 CBRs.
(G) DNA FISH on a terminal CBR from chromosome 6.
(H) DNA FISH on a terminal CBR from chromosome 12.

Scale bars, 5 μm. See also Figure S7.

ends during *Ascaris* DNA elimination. Thus, *Ascaris* chromosomes undergo comprehensive end remodeling during DNA elimination.

Eliminated DNA

Previous work demonstrated that the eliminated DNA consisted primarily of a tandem 120 bp repeat and unique sequences including 1,000 genes [14, 20]. The new chromosome assemblies indicate that the eliminated 120 bp tandem repeat constitutes ~30 Mb of DNA, 10% of the genome, and 54% of the eliminated DNA. This repetitive sequence is present in 25/48 of the chromosome ends that are eliminated and 9/12 of the internally eliminated regions of chromosome, but absent in all small internal eliminated regions. While the 120 bp tandem repeat is not present in all eliminated regions, genes are present in all regions of the genome eliminated. The size of the eliminated regions containing the 120 bp tandem repeat is a minimum length. The length of the tandem repeat was typically greater than the PacBio reads (on average 900 kb) and thus assembly across the repeat was not possible.

All chromosomes undergo remodeling of the ends of their chromosomes (Figure 2) with the loss of genes and repetitive sequences from these regions. The range of sequence lost from the ends of chromosomes is from 24 to 829 kb with an average length of 247 kb and a total of 11.5 Mb eliminated. Twelve internal regions of chromosomes are also eliminated (Figure 2), with a range of sequence lost from 43 kb to 1.6 Mb with an average length of 694 kb and a total of 8.3 Mb eliminated. Thus, while the size of the DNA eliminated from internal regions of chromosomes is on average larger than from the ends of the chromosomes, the total amount of DNA eliminated from the chromosome ends is much greater when including the 120 bp and subtelomeric repeats lost. Furthermore, while all chromosome ends are remodeled, only 11/24 chromosomes (8/19 autosomes and 3/5 sex chromosomes) undergo internal DNA elimination. We estimate the average length of the subtelomeric repeats is ~100 kb and the telomeres are ~15 kb. Overall, the eliminated DNA consists of 30 Mb 120 bp repeat, 11.5 Mb terminal deletion, 8.3 Mb internal deletion, and 5.5 Mb of subtelomeric and telomere repeats. Thus, the total amount of eliminated sequence is 55.3 Mb or 18% of the genome with a germline genome of ~308 Mb.

Internal CBRs Split 11 Germline Chromosomes into 23 Somatic Chromosomes

DNA breaks near the ends of all the chromosomes remove the subtelomeric and telomeric sequences, but do not contribute

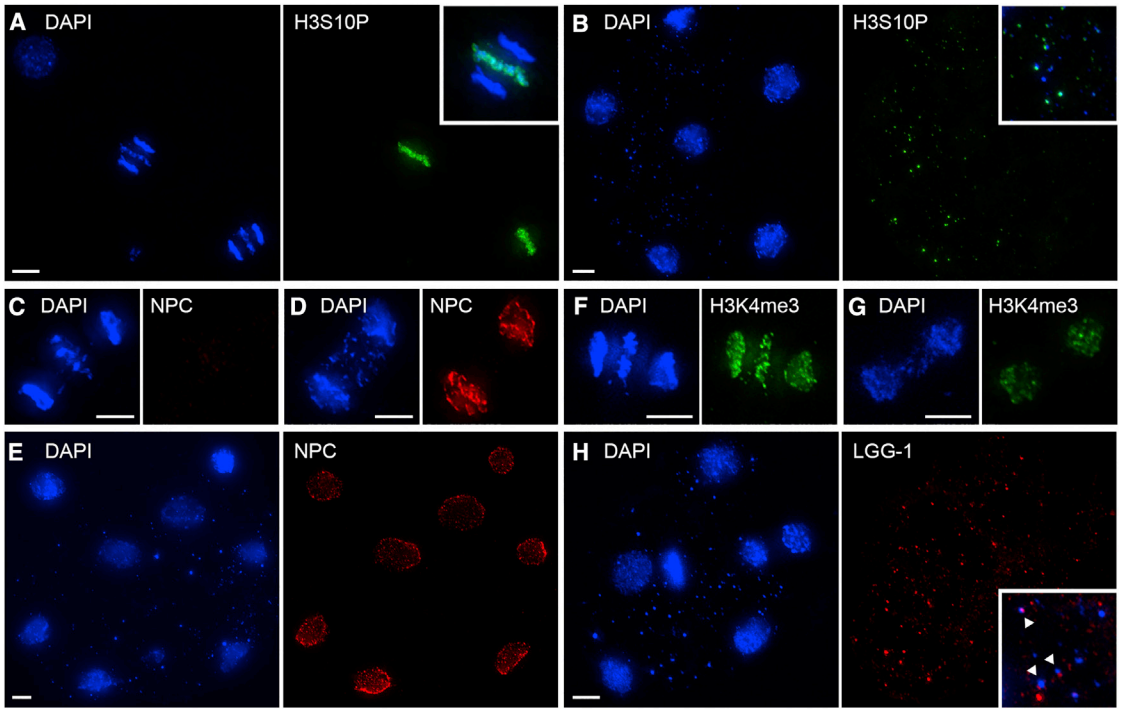

Figure 4. Eliminated DNA Is Marked with H3S10P, Localizes to the Cytoplasm, and Is Associated with Autophagosomes

(A) Anaphase of 4-cell DNA elimination mitosis. DAPI in blue and H3S10P IHC in green. The fourth cell nucleus is out of the image plane. Inset: merged DAPI and H3S10P IHC.

(B) Eliminated DNA fragments in the cytoplasm retain H3S10P. Six-cell stage with DAPI DNA fragments in cytoplasm (left panel) and higher magnification of DNA fragments with H3S10P IHC in right panel and in the merged inset. Note that not all DNA fragments in the cytoplasm show H3S10P staining. Chromosomes at prophase prior to a DNA elimination do not exhibit uniform H3S10P staining of chromosomes (Figure S4A).

(C–E) Nuclear pore complex (NPC) IHC during a DNA elimination telophase. Note that the NPC, absent during anaphase (C), is present in daughter nuclei forming in (D) and in the nuclei of the eight-cell stage in (E), but that eliminated DNA in micronuclei do not exhibit NPCs (see also EM text below).

(F and G) H3K4me3 IHC shows no differential staining between segregated and eliminated material in DNA elimination anaphase of 4-cell embryo (F) but is depleted from eliminated DNA at telophase (G).

(H) LGG-1 IHC in an 8-cell embryo suggests DNA containing membrane-bound structures in the cytoplasm form autophagosomes (inset, arrowheads). DAPI staining in left panel, LGG-1 IHC in right panel, and inset zoom of merged DAPI and LGG-1 IHC.

Scale bars, 5 μm. See also Figure S4.

to changes in chromosome number. Twenty-four internal CBRs in 11 chromosomes split the germline chromosomes into 23 smaller somatic chromosomes (Figure 2; Table 1), thus increasing the number of autosomes from 19 in the germline to 27 in somatic cells and the number of sex chromosomes from 5 in the germline to 9 in somatic cells. The largest chromosome (X1) is broken into three somatic chromosomes whereas the other 10 germline chromosomes are split into 2 somatic chromosomes. To determine if there are any features that distinguish the internal versus terminal CBRs, we carried out DNA motif, ATAC-seq, and other analyses on these two types of CBRs. No distinctive features were identified between these two types of CBRs and both become similarly more chromatin accessible for DNA elimination (Figure S2). Overall, while the internal chromosome breaks contribute to the increased somatic chromosome number, there are no differences in characteristics between the internal and terminal CBRs.

Histone Changes during DNA Elimination

During a DNA elimination mitosis, DNA that will be eliminated initially remains at the metaphase plate and is not segregated during anaphase (Figure 4A). Following telophase and cytokinesis, this DNA localizes to the cytoplasm, where it is eventually degraded (Figure 4B). To further examine DNA elimination mitoses and the fate of eliminated DNA, we conducted light and EM analyses. We first asked whether DNA that was destined for elimination at anaphase of an elimination mitosis exhibited different histone marks compared to DNA that would be retained. Immunohistochemical (IHC) analysis of several active and repressive histone marks (H3K4me1/3, H3K9me2/3, H3K36me2/3, H4K16ac, and H3K27me3) during anaphase of a DNA elimination indicated no clear differences between retained versus eliminated DNA (Figure S4C). However, H3S10P preferentially marked eliminated DNA (Figures 4A and 4B) and H2AK119ub (Figure S4B) was reduced in the eliminated DNA during anaphase of a DNA elimination. Histone H3S10P remains on the DNA that is relegated to the cytoplasm. At telophase of a DNA elimination mitosis, active histone marks (H3K4me3 and H4K16ac; Figures 4F, 4G, and S4B) are lost on the eliminated DNA. The eliminated DNA in the cytoplasm disappears over time and is gone after several cell divisions. To determine whether autophagy might be involved in the degradation and

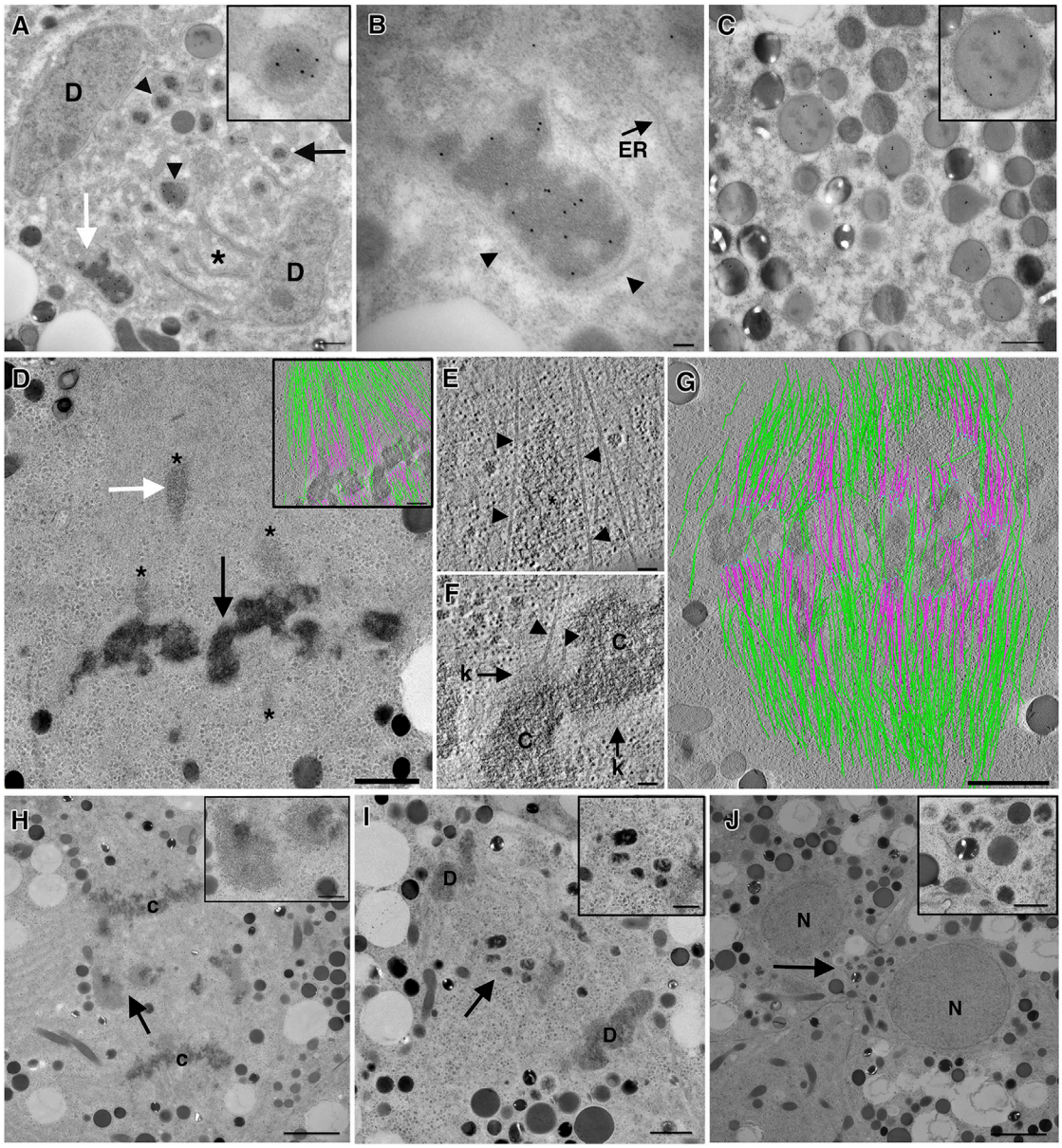

Figure 5. Electron Microscopy Provides an Ultrastructural Timeline of *Ascaris* DNA Elimination

(A–C) Immuno-EM using an antibody to H3S10P and a secondary antibody coupled to 15 nm gold identifies double membrane-bound structures containing DNA.

(A) Telophase cell in a DNA elimination mitosis. Nuclear envelope surrounds segregated DNA at the spindle poles (D) (see also I). Numerous membrane-bound organelles containing electron-dense material label with this antibody (arrowheads; black arrow points to granule surrounded by double membrane in inset; white arrow points to granule shown at higher magnification in B). Scale bar, 500 nm. Membrane compartments containing dense material (above and below the star) were also observed spanning the region of DNA elimination.

(B) H3S10P antibody preferentially labels dense material within double membrane-bound organelles (black arrowheads). ER, endoplasmic reticulum. Scale bar, 100 nm.

(C) H3S10P antibody labels numerous structures in the cytoplasm of post-diminution cells. Scale bar, 500 nm.

(D–G) Late prometaphase of a DNA elimination mitosis at the 4-cell stage.

(D) Overview shows darkly stained, condensed chromosomes at the metaphase plate. Lighter staining chromatin (*) was observed in the spindle proper and close to the metaphase plate. Scale bar, 1 μm. Inset shows a model from a tomographic volume computed from two serial sections (green, MTs that do not end on chromatin or go out of the reconstructed volume; purple, KMTs that end on the chromosomes). Serial, tomographic slices and projected 3D model from this region are shown in Video S1. White and black arrows indicate regions from selected tomographic slices shown in (E) and (F), respectively.

(E) Tomographic slice showing fine structure of the lighter staining, diffuse chromatin in the spindle (white arrow in D). Kinetochores were not observed on this diffuse chromatin, but it was always surrounded by numerous MTs in close, lateral proximity (arrowheads; scale bar, 100 nm). Serial, tomographic slices showing modeled MTs are shown in Video S2.

(legend continued on next page)

elimination of the cytoplasmic DNA, we used an antibody against a *C. elegans* marker for autophagosomes LGG-1 [34, 35], an ortholog of Atg8/LC3 protein involved in autophagy [36]. LGG-1 IHC staining in *Ascaris* embryos (Figure 4H) shows distinct LGG-1 puncta, similar to patterns observed in *C. elegans* embryos [34, 37, 38], and these puncta are coincident with DNA and H3S10P membrane-bound structures (see Figure 5 below), suggesting that eliminated DNA degradation likely occurs through autophagy. Overall, our data suggest that the eliminated DNA undergoes dynamic changes over time and its degradation involves autophagy.

Eliminated DNA Is Packaged into Double Membrane-Bound Structures (Micronuclei)

EM of DNA elimination mitoses identified numerous double membrane-bound structures of heterogeneous size and shape in telophase cells (Figures 5A–5C). These structures appear when the nuclear membrane reforms around the retained daughter nuclear DNA and are present in the cytoplasm of cells that have undergone DNA elimination (Figure 5C). Immuno-EM (using an antibody to H3S10P) demonstrated that the telophase structures and those present in the cytoplasm following DNA elimination were positive for H3S10P, indicating the presence of chromatin. These results indicate that the eliminated DNA is compartmentalized into double membrane-bound structures (Figures 5A–5C, insets; Figures S5A and S5B). Overall, the structures have characteristics of micronuclei and will hereafter be called micronuclei [39]. The H3S10P antibody preferentially labeled electron-dense material within the core of the structures, indicating the material is hyper-condensed DNA (Figure 5B). In addition, the cytoplasm of cells after DNA elimination contained numerous structures that labeled with the H3S10 antibody (Figure 5C). No labeling was detected on control sections (Figure S5C and S5D). Consistent with what was observed by IHC, the H3S10P antibody did not label DNA that had segregated to daughter nuclei (Figures 4 and 5A). Notably, based on IHC and EM, the micronuclei have limited or no nuclear pore complexes (Figures 4C–4E and 5).

Ultrastructural Timeline of DNA Elimination

We next used EM to study the timeline of DNA elimination. Late prometaphase spindles contain highly condensed chromosomes at the metaphase plate (Figure 5D). Surprisingly, lighter staining, more diffuse chromatin was observed near the metaphase plate and in the body of each half-spindle (Figure 5D, *). Electron tomography of adjacent sections was performed to characterize the 3D organization of spindle microtubules (MTs), both at the condensed chromosomes and the lighter stained, more diffuse chromatin (Figure 5D, inset model). Shown in this model and in Video S1, 115 MTs were identified as kinetochore microtubules (KMTs) that made end-on attachments to kinetochores on condensed chromosomes (Figure 5D, purple; Video S1). Such structures and connections were only found on condensed chromosomes. The other 345 MTs tracked (Figure 5D, green; Video S1) were identified as non-KMTs; these either did not end on chromosomes or went out of the volume of the reconstruction. These non-KMTs surround the regions containing diffuse chromatin but do not make end-on attachments (Video S1). The diffuse chromatin in the half-spindles was structurally different from the highly condensed chromosomes at the metaphase plate (compare Figures 5E and 5F) and appeared more lightly stained and less compact. Tomographic reconstructions revealed that this material does not assemble kinetochores and does not contain MT end-on attachments. Instead, MTs pass this material, making close, lateral contacts (Figure 5E, arrowheads; Video S2). In contrast, the highly condensed chromosomes at the metaphase plate appear more compact and assemble clear kinetochores to which KMTs attach (Figure 5F). Figure S6 and Video S3 show that even when diffuse chromatin was situated near condensed chromosomes, only the condensed chromosomes assemble kinetochores and have KMTs. A larger tomographic volume was computed from a different region of the prometaphase spindle. Of the 663 MTs tracked, 187 were identified as KMTs (Figures 5G, S6C, and S6D, purple; Video S4) that were only at the condensed chromosomes. Again, there were no recognizable kinetochores or end-on attachments of MTs (green; n = 476) to the diffuse, less condensed chromatin present in the volume (Figure 5G, green; Video S4). These data demonstrate that there are two distinguishable forms of chromatin condensation, one of which leads to normal chromosomes whereas the other leads to chromatin masses that do not assemble kinetochores or bind to KMTs. This diffuse, less condensed chromatin that will be eliminated can be distinguished ultrastructurally from the condensed chromosomes and can be identified in the spindle prior to metaphase.

EM of DNA elimination anaphase spindles shows segregated chromosomes near the spindle poles and eliminated DNA remaining at the spindle midplane (Figure 5H, c's and arrow, respectively). The eliminated DNA at the spindle midplane was not attached to MTs and appeared as masses of diffuse chromatin similar in structure to that observed in prometaphase (Figure 5H, inset). This material was not surrounded by membrane at this stage. The nuclear envelope begins to reform around

(F) In contrast, the highly condensed chromosomes (C) at the metaphase plate assemble kinetochores (k) that are associated with KMTs (arrowheads). Scale bar, 100 nm. Video S3 and Figure S6 show serial, tomographic slices from another area showing KMTs at chromosomes, but not at the diffuse chromatin.
(G) 3D model of the MTs in 3 serial, 200 nm thick sections from the prometaphase spindle. KMTs (purple) end on condensed chromosomes only. Scale bar, 1 μm. Serial, tomographic slices and projected 3D model from this region are shown in Video S4.
(H and I) Double membranes begin to surround eliminated DNA at telophase.
(H) Overview of a DNA elimination mitosis in anaphase shows segregated chromosomes (C) at each pole with eliminated DNA at the spindle equator. Arrow points to mass of lightly condensed material. Higher magnification (inset) shows that this material is not surrounded by membrane. Scale bar, 2 μm; inset bar, 500 nm.
(I) Membranes begin to surround eliminated DNA at telophase. Nuclear envelope begins to form around segregated DNA at the spindle poles (D's). Micronuclei containing eliminated DNA appear more darkly stained and are surrounded by double membranes (arrow, inset). Scale bar, 500 nm; inset bar, 500 nm.
(J) Cytokinesis following a DNA elimination mitosis shows two daughter nuclei (N) and numerous micronuclei near the spindle midbody (arrow, inset). Scale bar, 2 μm; inset bar, 500 nm.
See also Figure S5 and S6.

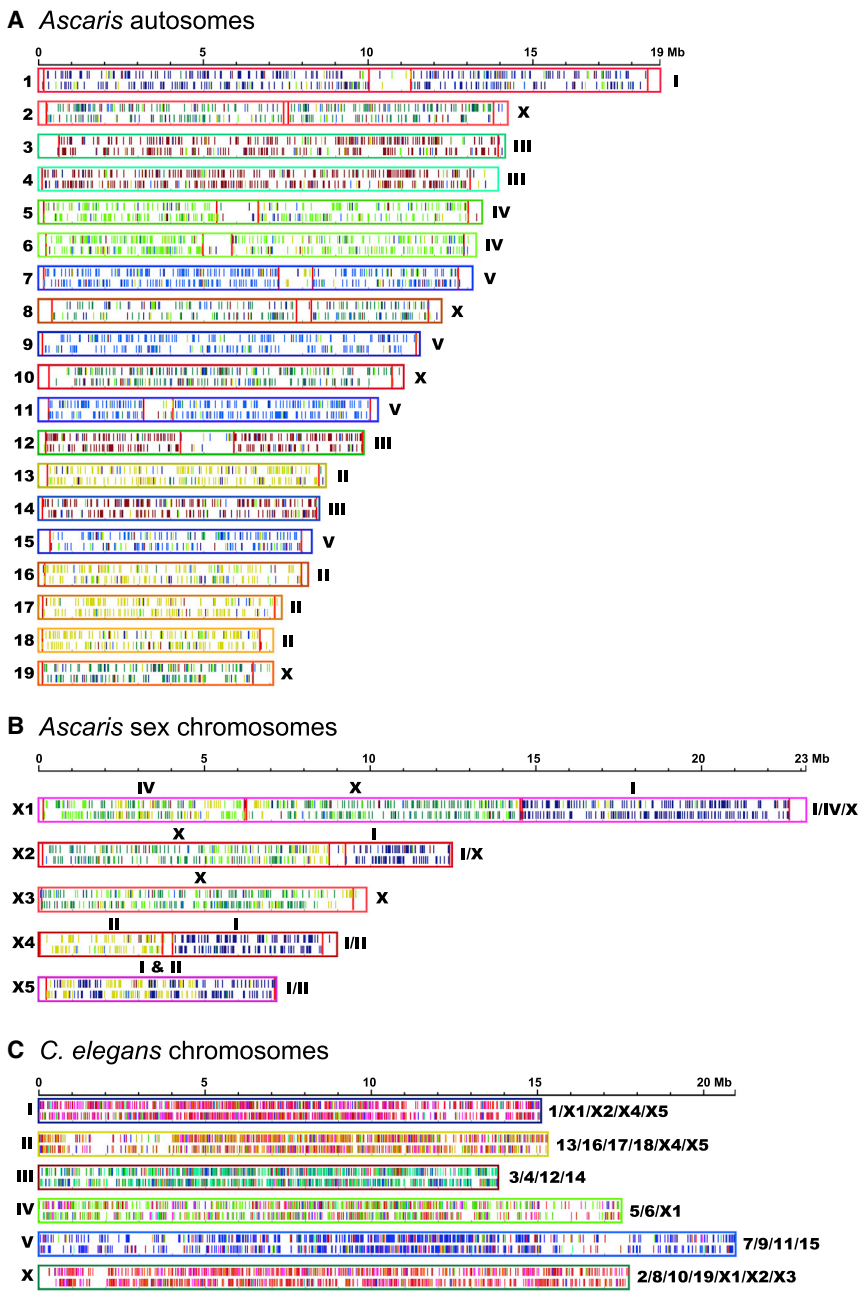

Figure 6. Comparison of *Ascaris* and *C. elegans* Chromosomes

The reciprocal best blast hits for orthologous *C. elegans* and *Ascaris* proteins (6,402) were identified and plotted on each chromosome. *C. elegans* and *Ascaris* chromosomes are each boxed with distinct colors. The color of the vertical bars in *Ascaris* chromosomes indicates the chromosome of origin in *C. elegans* (based on the *C. elegans* chromosome box color) and vice versa for *Ascaris* genes in *C. elegans* chromosomes. The top half vertical lines correspond to genes on the forward strand whereas the bottom vertical lines are genes on the reverse strand. The chromosomes are labeled on the left. On the right of each chromosome indicates the corresponding major chromosome of either *C. elegans* or *Ascaris*. The top of the *Ascaris* sex chromosomes also shows the orthologous *C. elegans* chromosome. Full vertical red lines in the *Ascaris* chromosomes indicate the chromosomal break regions where DNA breaks occur during DNA elimination. See Table S2 for all orthologous proteins and their chromosomal coordinates. Figure S6

segregated DNA at late anaphase/telophase (Figures 5A and 5I). Double membranes surrounding the eliminated DNA, micronuclei, are first observed at this stage (Figure 5I, inset; Figure 5A). The DNA in these structures becomes more condensed compared to the diffuse chromatin observed in prometaphase and anaphase. At cytokinesis, the micronuclei are observed near the cleavage furrow (Figure 5J, arrow). Overall, the EM data suggest that retained and eliminated DNA can be identified and differentiated with the diffuse, less condensed chromatin (DNA for elimination) appearing adjacent to the metaphase but without kinetochores or KMTs. DNA FISH for the eliminated 120 bp repeat (Figure S6) also shows that this eliminated DNA is adjacent to the metaphase plate.

Chromosome Fusion in *Ascaris* Sex Chromosomes

Ascaris has a large number of germline chromosomes [28] compared to most other known nematodes (most have 4–12 or less) [40]. To further examine *Ascaris* chromosomes, particularly the unusual multiple sex chromosomes, we compared the 24 *Ascaris* germline chromosomes to the 6 chromosomes in the free-living nematode *C. elegans*, which likely represents an ancestral chromosome state (Figure 6). All 19 *Ascaris* autosomes can be traced to an individual *C. elegans* chromosome; thus, the expansion of *Ascaris* autosomes is likely due to the subdivision of individual ancestral chromosomes (Figure 6). While in general gene linkage for these 19 autosomes is maintained between the two species, there is little overall chromosomal synteny. This suggests that there has been extensive genome rearrangement within chromosomes after the separation of the species, as seen in other nematodes [41–43]. In contrast, the majority of *Ascaris* sex chromosomes (X1, X2, X4, and X5) were traced to multiple *C. elegans* chromosomes (Figure 6B). While some rearrangements are present in chromosome X5, the three other *Ascaris* sex chromosomes (X1, X2, and X4) are devoid of rearrangement between the blocks of chromosomes, particularly for the blocks matching *C. elegans* chromosome I. This suggests that these *Ascaris* sex chromosomes are likely derived from recent chromosome fusion events. Interestingly, the boundaries for these fused chromosome blocks coincide with the *Ascaris* CBRs (Figure 6B). With the DNA breaks at the CBRs during DNA elimination, the *Ascaris*

sex chromosomes become orthologous to single *C. elegans* chromosomes following DNA elimination. Finally, the *Ascaris* eliminated DNA regions have very few unique orthologous genes to *C. elegans*, suggesting that these eliminated regions have recently evolved or are evolutionarily more flexible than the rest of the genome. These more flexible regions may readily enable the birth of new genes, consistent with the observation that novel genes are often enriched and expressed in the testis and also consistent with their propensity for elimination in *Ascaris* [44–46]. Overall, our comparative analysis of the *C. elegans* and *Ascaris* chromosomes reveals that many *Ascaris* sex chromosomes are the result of recent fusion events and that DNA elimination chromosome breaks re-subdivide these chromosomes into single chromosomes that are orthologous to individual ancestral chromosomes.

DISCUSSION

We describe significantly improved germline and somatic genome assemblies for the parasitic nematode *Ascaris* that provide novel insights into programmed DNA elimination. The full-chromosome assemblies provide the first and most comprehensive chromosomal view of DNA elimination in a metazoan. Comparison of these assemblies demonstrated that all germline chromosomes undergo breaks in subtelomeric regions with loss of distal sequences and healing of chromosome ends by *de novo* telomere addition. EM and IHC analyses indicate that eliminated DNA is packaged into double membrane-bound structures, which we call micronuclei, at telophase. These micronuclei undergo chromatin changes over time including the loss of active histone marks, localize to the cytoplasm, and become autophagosomes degrading the DNA. Comparative analysis of the *Ascaris* chromosomes suggests that *Ascaris* sex chromosomes were formed by chromosome fusions that are resolved into independent chromosomes through the DNA breaks at CBRs during DNA elimination. Our comprehensive genomic and cytological studies on DNA elimination provide key new insights into metazoan DNA elimination.

Remodeling of Chromosome Ends

DNA FISH for telomeres indicates telomeres are removed from all *Ascaris* chromosomes during DNA elimination, and subsequent telomere length extension was asynchronous, requiring several cell cycles, consistent with a previous study [28] (Figures 3 and S3). Our genome analyses indicate that during DNA elimination, subtelomeric chromosome breaks occur, releasing the distal portions of chromosome with their intact telomeres. Our subtelomeric DNA FISH experiments support that chromosomes undergo subtelomeric breaks and confirm the loss of distal chromosome regions and their telomeres during DNA elimination. Thus, all *Ascaris* germline chromosomes undergo chromosome end remodeling during DNA elimination (Figures 2, 3, and S3).

The new finding that all germline chromosome ends undergo remodeling through subtelomeric breaks and addition of *de novo* telomeres raises a variety of questions. For example, what impact does the remodeling have on chromosome architecture? Subdivision of single chromosomes into two or more chromosomes and the remodeling of the chromosome ends are likely to alter the overall architecture of each chromosome and inter-chromosome interactions. It remains to be determined what overall impact DNA elimination has on *Ascaris* chromosome architecture and whether the architecture prior to and during DNA elimination might contribute to DNA elimination as recently observed in the ciliate *Tetrahymena* [47]. An open question is whether the breaks in subtelomeric regions (and internal regions) are facilitated by chromosome looping mechanisms that contribute to the DNA breaks. Further high-resolution and stage-specific Hi-C and FISH work is needed to address these questions.

The remodeling of chromosome ends may also impact the overall gene expression of the chromosomes. Muller [48] first suggested that the chromosome breaks and addition of new telomeres may lead to a "telomere position effect" on gene expression following DNA elimination [49]. No pattern of gene silencing or activation was identified in previous studies on a single CBR [48] and within 50 kb of a number of CBRs [14] using steady-state RNA level analyses. Future comprehensive nascent RNA sequencing before, during, and after DNA elimination is required to determine if the all-inclusive chromosome end remodeling described here impacts gene expression near the ends of the newly remodeled chromosomes.

DNA Elimination of the *Ascaris* 120 bp Repeat

The majority of the eliminated DNA (54%) consists of a 120 bp tandem repeat, with over 99% of this repeat lost. The large amount of repeat eliminated has historically led to the speculation that the repeat may be mechanistically involved in the elimination process. Our new chromosome assemblies enabled us to identify the location of these repeats on the chromosomes and their proximity to the DNA breaks. The location of the 120 bp tandem repeats within the eliminated regions is variable, but typically not near where the chromosomal DNA breaks (CBRs) occur; the majority of the CBRs (50/72, 70%) are not within 200 kb of the repeats. This suggests it is unlikely the 120 bp repeats play a direct role in the DNA breaks and DNA elimination. However, we cannot rule out that the repeats may contribute to some higher-order 3D chromosome organization that contributes to DNA elimination. Notably, not all eliminated genome regions contain the 120 bp tandem repeat. However, all eliminated genome regions contain genes. This suggests that the loss of genes is not simply a consequence of being linked to regions of the genome where the 120 bp tandem repeat is located. Thus, *Ascaris* DNA elimination serves not to just simply remove the 120 bp repeats. The findings support our model that the elimination of genes is a key component of DNA elimination [14, 20].

DNA Breaks

Analysis of all the sites for DNA breaks (including 32 new sites in the current study) further supports that there are no sequence, structural motifs, histone marks, small RNAs, or other features that define or target the 3–6 kb CBRs as sites for the chromosome DNA breaks that occur during DNA elimination [14, 20–23]. Overall, these characteristics suggest it is unlikely a sequence-specific endonuclease is involved in generating the DNA breaks. However, we cannot rule out that an enzyme similar to a Type I restriction enzyme [50] that recognizes unique sequences at a distance from the CBRs might be involved.

Domesticated transposases, such as RAG1-RAG2 for V(D)J recombination [51–53] and PiggyBac in ciliate DNA elimination [54–57], recognize specific sequences in the genome during development to generate double-strand DNA breaks. However, we have not identified any transposases or their signatures in *Ascaris* that might generate the DNA elimination chromosome breaks. In ciliates, programmed DNA rearrangements involve the elimination of short internal sequences followed by re-ligation of the boundaries (IES) and many chromosomal break sites (CBSs) that lead to new chromosomes and loss of sequences [15–19, 58]. While there is some understanding of the DNA breaks at IESs, the mechanism for the CBS is unknown. Thus, the mechanism(s) for key DNA breaks in DNA elimination remain unknown. The open chromatin we identified at the CBRs likely contributes to identification of regions for the *Ascaris* breaks, facilitates the generation of the breaks, and/or is a consequence of molecular processes that contribute to the generation of the breaks [14].

Compartmentalization of Eliminated DNA into Micronuclei during Telophase

Using improved methods for EM specimen preparation [59–61], we observed two distinguishable forms of chromatin condensation: one leads to normal chromosomes whereas the other leads to chromatin masses that are less diffuse and compact. The diffuse, less condensed chromatin destined for elimination can be identified near the metaphase plate and in the spindle proper in late prometaphase. Electron tomography confirmed that this material does not assemble a kinetochore or make end-on connections with KMTs; it is instead surrounded by lateral MTs. This is consistent with reduced CENP-A in chromosome regions that will be lost in *Ascaris* DNA elimination [26] (this study) and EM studies in *Parascaris* [24, 25]. Notably, DNA FISH (Figure S7) indicates that the eliminated 120 bp repeat is present at the boundary of the metaphase plate. Furthermore, previous studies suggested that chromosome DNA destined for elimination in both *Ascaris* and *Parascaris* was less condensed [28]. Overall, these data show that DNA to be eliminated undergoes differential condensation and is often situated at the boundary of the metaphase plate. This diffuse chromatin is not segregated in anaphase, remaining in the spindle midplane as retained chromosomes move to the poles. Concurrent with nuclear envelope reformation at telophase, the eliminated DNA is surrounded by a double membrane at telophase, forming structures similar to micronuclei. During telophase and cytokinesis, the DNA within the micronuclei becomes more condensed, which may be related to the loss of active histone marks. These micronuclei persist in the cytoplasm following the end of a DNA elimination mitosis for some time and eventually disappear. The EM studies presented thus provide new details of mitotic spindle organization and further our understanding of the ultrastructural timeline of DNA elimination in *Ascaris*.

During mitosis, H3S10P marks chromosomes for condensation and is removed as anaphase progresses [62]. We observed that DNA to be eliminated that remains at the metaphase plate contained high levels of histone H3S10P whereas segregated and retained DNA did not (Figures 4 and 5). We suggest that the DNA to be eliminated does not undergo the metaphase to anaphase transition, thus retaining H3S10P [63, 64]. Notably, eliminated DNA (Figures 3 and 5) is incorporated into micronuclei at telophase, localizes to the cytoplasm, and is eventually degraded. Thus, eliminated DNA is sequestered into micronuclei at telophase during a DNA elimination and also undergoes changes in histone modifications (Figures 4 and S4). The micronuclei have significantly reduced nuclear pore complexes (Figures 4 and 5).

Micronuclei have been described associated with DNA elimination in lampreys, the cartilaginous rat fish, and water frogs [5, 11, 12, 65]. EM studies in water frogs and the rat fish provide structural evidence for micronuclei demonstrating double membrane-bound vesicles. Micronuclei in water frogs exhibited fewer nuclear pore complexes and greater heterochromatinization than the main nuclei. In lampreys, micronuclei did not possess lamin B1 or nuclear pore O-linked glycoproteins. Thus, eliminated DNA appears to be incorporated into micronuclei-like vesicles in all these organisms. The micronuclei-like vesicles in the cytoplasm of *Ascaris* embryos show association with LGG-1 puncta suggestive of different stages of autophagosome formation (Figure 4H). Similar associations have been observed in DNA elimination events in water frogs [5] and the ciliate *Tetrahymena* [66], and autophagy has been shown to play a role following meiosis in the programmed nuclear death of the old macronucleus in *Tetrahymena*. In the copepod, *Cyclops kolensis*, eliminated DNA is present in double membrane-bound structures late in interphase and early prophase of an elimination division [67]. We recently observed similar double membrane-bound structures in another copepod, *Mesocyclops edax* (M.Z., E.T.O., and R.E.D., unpublished data), where DNA "droplets" were described [68]. In *C. kolensis*, the double membrane-bound structures increase in size, speculated to result from fusion of the structures, and the double membrane is reduced to a poreless single membrane by late telophase. These structures with the DNA become cytoplasmic and are rapidly degraded.

Timing of DNA Breaks

Previous models for *Ascaris* DNA elimination postulated that the DNA breaks likely occurred at the metaphase plate during an elimination mitosis [28]. Our previous data indicate that chromosome regions that will be lost have reduced CENP-A and kinetochores prior to a DNA elimination mitosis [26]. If the DNA breaks occurred prior to mitosis, some alternative mechanism would be required to congress eliminated chromosome fragments to the metaphase plate. The EM structural data described here suggest there are chromosome fragments at the boundary of the metaphase plate during a DNA elimination mitosis that do not have kinetochores or KMTs attached. This suggests that DNA breaks in the chromosomes may have occurred prior to metaphase. Strikingly, preliminary END-seq data [69] to define the timing and the sites of *Ascaris* DNA breaks suggest that the DNA breaks may occur prior to the mitosis of a DNA elimination (J.W. and R.E.D., unpublished data). In addition, DNA FISH for the eliminated 120 bp repeat indicates this DNA localizes adjacent to the metaphase plate during a DNA elimination. Thus, these data suggest that the DNA elimination breaks likely occur prior to mitosis. Our EM observations clearly indicate that the eliminated DNA must reach the metaphase plate through mechanisms that are independent of kinetochores and KMTs. Remarkably, studies in *C. elegans* have shown that chromosomes

congress to the spindle midplane after depletion of kinetochore complex proteins using RNAi, although these chromosomes remain disorganized and are not segregated [70, 71]. Thus, alternative mechanisms for congression of the eliminated DNA to the metaphase plate must be involved since the DNA lacks CENP-A and kinetochores [26]. These mechanisms could include the contribution of polar ejection forces involving dynamic instability of pole-initiated MTs, plus-end directed chromokinesins, the contribution of interpolar microtubules, or scaffolding or tethering proteins within the spindle [72–77].

Ascaris Sex Chromosome Fusions and Their Separation in Somatic Cells by DNA Elimination

Nematodes typically have a small number of chromosomes (4–12) [40]. Assuming that the Clade V free-living *C. elegans* and *Pristionchus pacificus* [33] represent an ancestral chromosome state with six chromosomes, our chromosome comparisons indicated that all of the *Ascaris* autosomes are likely independent regions of these ancestral chromosomes (Figure 6). In contrast, several *Ascaris* germline sex chromosomes appear to be fusions of independent regions of ancestral chromosomes (also defined by using Nigon elements in other studies [78, 79]) (Figure 6B). These fused chromosomes become independent chromosomes in somatic cells after DNA elimination as the regions are separated by CBRs that break the chromosomes. Extreme fusion of chromosomes appears to have occurred in some ascarids where the complete germline genome becomes a single chromosome as in *Parascaris univalens*. Notably, following DNA elimination, this single *P. univalens* germline chromosomes is subdivided into 35 somatic chromosomes (29 autosomes and 6 sex chromosomes) [28]. Thus, while the fusion of chromosomes may be accommodated in the germline genome, their separation by DNA elimination chromosome breaks may be necessary in somatic cells. Overall, we suggest that *Ascaris* ancestral chromosomes may have undergone multiple breaks to form many smaller chromosomes. These chromosomes recently fused to form multiple germline sex chromosomes, only to be separated in somatic cells during DNA elimination (5 in germline cells and 9 in somatic cells). An open question is why sex chromosomes are increased and separated in somatic cells compared to germ cells.

DNA Elimination in Other Organisms

In ciliates, formation of macronuclear chromosomes (somatic genome) results from many chromosome breaks in the micronuclear chromosomes (germline) and the healing of the broken ends by telomere addition. In *Tetrahymena thermophila*, for example, 225 chromosome break sites in the 5 germline chromosomes lead to 181 small amplified (~45 copies on average 900 kb chromosomes) macronuclear chromosomes (somatic) [80]. The chromosome end remodeling observed in *Ascaris* differs from that described in ciliates in that the breaks do not generate a large number of relatively small chromosomes and no amplification occurs.

In copepods, large amounts of DNA are eliminated while chromosome numbers, in general, do not change [7, 67]. One model for DNA elimination in copepods is that internal elimination within chromosomes involves looping out of DNA, excision of the DNA, and ligation of the ends. However, the contribution of internal versus terminal DNA elimination remains unknown. Programmed DNA elimination in lampreys is associated with decreased chromosome numbers (chromosome loss and/or fusion) and loss of ~20% the germline DNA (500 Mb DNA) in somatic cells, both repetitive sequences, and some germline expressed genes [9, 10, 12, 13]. In hagfish, to date, loss of only repetitive sequences has been identified [2, 8]. DNA FISH and cytogenetic analysis indicate the loss of whole hagfish chromosomes and chromosome termini encompassing 21%–75% of the germline DNA in different species [2, 8]. It is not known whether the loss at hagfish chromosome termini is similar to that observed here in *Ascaris* or if an excision event (internal deletion and fusion) occurs removing subtelomeric regions without loss of the telomere from the chromosome.

Conclusions

Programmed DNA elimination occurs in diverse organisms from ciliates to vertebrates. Here, we have generated complete chromosome assemblies of all *Ascaris* germline and somatic chromosomes. Comparison of these assemblies provides the first chromosome view of metazoan DNA elimination including the location of all DNA breaks and the locations of eliminated sequences including repeats and genes. The predominant DNA elimination events in *Ascaris* are comprehensive chromosome end remodeling through breaks in the subtelomeres of all 24 germline chromosomes, loss of distal chromosome sequences, and healing of the breaks by *de novo* telomere addition. The major eliminated sequence, a 120 bp satellite repeat (30 Mb), is not present in all eliminated regions of the genome. All eliminated DNA contains genes (~1,000 genes in total) that are predominantly expressed in the germline. We provide an ultrastructural timeline for a DNA elimination mitosis and describe the incorporation of eliminated DNA into double membrane-bound structures, micronuclei, at telophase. Chromatin in these micronuclei exhibit loss of active histone marks and appear to be degraded through autophagy. Our data also suggest recent chromosome fusions in the germline that are broken into multiple sex chromosomes during DNA elimination. These studies provide the most comprehensive genome analysis of DNA elimination in a metazoan, an ultrastructural analysis of DNA elimination, and identify additional novel and key aspects of metazoan DNA elimination.

STAR★METHODS

Detailed methods are provided in the online version of this paper and include the following:

- KEY RESOURCES TABLE
- RESOURCE AVAILABILITY
  - Lead Contact
  - Materials Availability
  - Data and Code Availability
- EXPERIMENTAL MODEL AND SUBJECT DETAILS
- METHOD DETAILS
  - *Ascaris* and megabase-size DNA isolation
  - PacBio sequencing and initial assembly
  - Hi-C data and scaffolding

- Genes and their tissue-specific expression analysis
- Repetitive sequence identification
- Antibodies and immunohistochemistry
- DNA FISH Probes
- DNA FISH
- Image acquisition
- Preparation of *Ascaris* embryos for electron microscopy
- Serial section electron microscopy, immuno-EM and electron tomography

SUPPLEMENTAL INFORMATION

Supplemental Information can be found online at https://doi.org/10.1016/j.cub.2020.06.058.

ACKNOWLEDGMENTS

We thank Bruce Bamber, Jeff Myers, and Routh Packing Co. for their support and hospitality in collecting *Ascaris* material. We thank Garry Morgan and Thomas Giddings for assistance with specimen preparation and immuno-EM experiments, the University of Colorado at Boulder EM Services Core Facility, and Thorsten Hoppe for generously providing the *C. elegans* Lgg-1 antibody. We thank Maggie Balas for her initial work on histone modification marks in *Ascaris* and *Parascaris* embryos; Dick Mcintosh for his interest, insight, and feedback on this work; and Rachel Patton McCord for interpretation of the Hi-C data. J.W. is supported by the University of Tennessee Knoxville Startup Funds. This work was supported by NIH grants to R.E.D. (AI114054) and J.W. (AI125869).

AUTHOR CONTRIBUTIONS

J.W. and R.E.D. designed the project; J.W. and R.E.D. prepared agarose plugs and megabase size genomic DNA; Y.K. and J.W. carried out the Hi-C experiments; J.W. and M.Z. carried out bioinformatic analyses; G.M.B.V. designed and carried out the DNA FISH and IHC; E.T.O.T. designed and carried out the EM analyses; J.W., G.M.B.V., M.Z., E.T.O.T., and R.E.D. analyzed data; and J.W., E.T.O.T., and R.E.D. wrote the manuscript.

DECLARATION OF INTERESTS

The authors declare no competing interests.

Received: April 30, 2020
Revised: June 9, 2020
Accepted: June 16, 2020
Published: July 16, 2020

REFERENCES

1. Wang, J., and Davis, R.E. (2014). Programmed DNA elimination in multicellular organisms. Curr. Opin. Genet. Dev. *27*, 26–34.
2. Kohno, S.-H., Kubota, S., and Nakai, Y. (1998). Chromatin diminution and chromosome elimination in hagfishes. In The Biology of Hagfishes, J.M. Jorgensen, J.P. Lomholt, R.E. Weber, and H. Malte, eds. (Chapman & Hall).
3. Streit, A., Wang, J., Kang, Y., and Davis, R.E. (2016). Gene silencing and sex determination by programmed DNA elimination in parasitic nematodes. Curr. Opin. Microbiol. *32*, 120–127.
4. Torgasheva, A.A., Malinovskaya, L.P., Zadesenets, K.S., Karamysheva, T.V., Kizilova, E.A., Akberdina, E.A., Pristyazhnyuk, I.E., Shnaider, E.P., Volodkina, V.A., Saifitdinova, A.F., et al. (2019). Germline-restricted chromosome (GRC) is widespread among songbirds. Proc. Natl. Acad. Sci. USA *116*, 11845–11850.
5. Chmielewska, M., Dedukh, D., Haczkiewicz, K., Rozenblut-Kościsty, B., Kaźmierczak, M., Kolenda, K., Serwa, E., Pietras-Lebioda, A., Krasikova, A., and Ogielska, M. (2018). The programmed DNA elimination and formation of micronuclei in germ line cells of the natural hybridogenetic water frog Pelophylax esculentus. Sci. Rep. *8*, 7870.
6. Lavanchy, G., and Schwander, T. (2019). Hybridogenesis. Curr. Biol. *29*, 539.
7. Grishanin, A. (2014). Chromatin diminution in Copepoda (Crustacea): pattern, biological role and evolutionary aspects. Comp. Cytogenet. *8*, 1–10.
8. Kojima, N.F., Kojima, K.K., Kobayakawa, S., Higashide, N., Hamanaka, C., Nitta, A., Koeda, I., Yamaguchi, T., Shichiri, M., Kohno, S., and Kubota, S. (2010). Whole chromosome elimination and chromosome terminus elimination both contribute to somatic differentiation in Taiwanese hagfish Paramyxine sheni. Chromosome Res. *18*, 383–400.
9. Smith, J.J., Baker, C., Eichler, E.E., and Amemiya, C.T. (2012). Genetic consequences of programmed genome rearrangement. Curr. Biol. *22*, 1524–1529.
10. Smith, J.J., Timoshevskaya, N., Ye, C., Holt, C., Keinath, M.C., Parker, H.J., Cook, M.E., Hess, J.E., Narum, S.R., Lamanna, F., et al. (2018). The sea lamprey germline genome provides insights into programmed genome rearrangement and vertebrate evolution. Nat. Genet. *50*, 270–277.
11. Stanley, H.P., Kasinsky, H.E., and Bols, N.C. (1984). Meiotic chromatin diminution in a vertebrate, the holocephalan fish Hydrolagus collie (Chondrichthyes, Holocephali). Tissue Cell *16*, 203–215.
12. Timoshevskiy, V.A., Herdy, J.R., Keinath, M.C., and Smith, J.J. (2016). Cellular and molecular features of developmentally programmed genome rearrangement in a vertebrate (sea lamprey: Petromyzon marinus). PLoS Genet. *12*, e1006103.
13. Timoshevskiy, V.A., Lampman, R.T., Hess, J.E., Porter, L.L., and Smith, J.J. (2017). Deep ancestry of programmed genome rearrangement in lampreys. Dev. Biol. *429*, 31–34.
14. Wang, J., Gao, S., Mostovoy, Y., Kang, Y., Zagoskin, M., Sun, Y., Zhang, B., White, L.K., Easton, A., Nutman, T.B., et al. (2017). Comparative genome analysis of programmed DNA elimination in nematodes. Genome Res. *27*, 2001–2014.
15. Allen, S.E., and Nowacki, M. (2020). Roles of noncoding RNAs in ciliate genome architecture. J. Mol. Biol. Published online January 10, 2020. https://doi.org/10.1016/j.jmb.2019.12.042.
16. Betermier, M., and Duharcourt, S. (2014). Programmed rearrangement in ciliates: paramecium. Microbiol. Spectr. *2*, https://doi.org/10.1128/microbiolspec.MDNA3-0035-2014.
17. Bracht, J.R., Fang, W., Goldman, A.D., Dolzhenko, E., Stein, E.M., and Landweber, L.F. (2013). Genomes on the edge: programmed genome instability in ciliates. Cell *152*, 406–416.
18. Noto, T., and Mochizuki, K. (2017). Whats, hows and whys of programmed DNA elimination in *Tetrahymena*. Open Biol. *7*, 170172.
19. Rzeszutek, I., Maurer-Alcalá, X.X., and Nowacki, M. (2020). Programmed genome rearrangements in ciliates. Cell. Mol. Life Sci. Published online May 27, 2020. https://doi.org/10.1007/s00018-020-03555-2.
20. Wang, J., Mitreva, M., Berriman, M., Thorne, A., Magrini, V., Koutsovoulos, G., Kumar, S., Blaxter, M.L., and Davis, R.E. (2012). Silencing of germline-expressed genes by DNA elimination in somatic cells. Dev. Cell *23*, 1072–1080.
21. Bachmann-Waldmann, C., Jentsch, S., Tobler, H., and Müller, F. (2004). Chromatin diminution leads to rapid evolutionary changes in the organization of the germ line genomes of the parasitic nematodes A. suum and P. univalens. Mol. Biochem. Parasitol. *134*, 53–64.
22. Jentsch, S., Tobler, H., and Müller, F. (2002). New telomere formation during the process of chromatin diminution in Ascaris suum. Int. J. Dev. Biol. *46*, 143–148.
23. Müller, F., Wicky, C., Spicher, A., and Tobler, H. (1991). New telomere formation after developmentally regulated chromosomal breakage during

the process of chromatin diminution in Ascaris lumbricoides. Cell *67*, 815–822.

24. Goday, C., Ciofi-Luzzatto, A., and Pimpinelli, S. (1985). Centromere ultrastructure in germ-line chromosomes of Parascaris. Chromosoma *91*, 121–125.
25. Goday, C., González-García, J.M., Esteban, M.R., Giovinazzo, G., and Pimpinelli, S. (1992). Kinetochores and chromatin diminution in early embryos of Parascaris univalens. J. Cell Biol. *118*, 23–32.
26. Kang, Y., Wang, J., Neff, A., Kratzer, S., Kimura, H., and Davis, R.E. (2016). Differential chromosomal localization of centromeric histone CENP-A contributes to nematode programmed DNA elimination. Cell Rep. *16*, 2308–2316.
27. Koren, S., Walenz, B.P., Berlin, K., Miller, J.R., Bergman, N.H., and Phillippy, A.M. (2017). Canu: scalable and accurate long-read assembly via adaptive *k*-mer weighting and repeat separation. Genome Res. *27*, 722–736.
28. Niedermaier, J., and Moritz, K.B. (2000). Organization and dynamics of satellite and telomere DNAs in Ascaris: implications for formation and programmed breakdown of compound chromosomes. Chromosoma *109*, 439–452.
29. Easton, A.V., Gao, S., Lawton, S.P., Khan, A., Dahlstrom, E., Oliveira, R.G., Kepha, S., Porcella, S.F., Webster, J.P., Anderson, R.M., et al. (2020). Extensive hybridization between pig and human Ascaris identifies a highly interbred species complex infecting humans. bioRxiv. https://doi.org/10.1101/2020.04.17.047407.
30. Jourdan, P.M., Lamberton, P.H.L., Fenwick, A., and Addiss, D.G. (2018). Soil-transmitted helminth infections. Lancet *391*, 252–265.
31. C. elegans Sequencing Consortium (1998). Genome sequence of the nematode C. elegans: a platform for investigating biology. Science *282*, 2012–2018.
32. Prabh, N., Roeseler, W., Witte, H., Eberhardt, G., Sommer, R.J., and Rödelsperger, C. (2018). Deep taxon sampling reveals the evolutionary dynamics of novel gene families in *Pristionchus* nematodes. Genome Res. *28*, 1664–1674.
33. Rödelsperger, C., Meyer, J.M., Prabh, N., Lanz, C., Bemm, F., and Sommer, R.J. (2017). Single-molecule sequencing reveals the chromosome-scale genomic architecture of the nematode model organism Pristionchus pacificus. Cell Rep. *21*, 834–844.
34. Lu, Q., Wu, F., and Zhang, H. (2013). Aggrephagy: lessons from C. elegans. Biochem. J. *452*, 381–390.
35. Zhang, H., Chang, J.T., Guo, B., Hansen, M., Jia, K., Kovács, A.L., Kumsta, C., Lapierre, L.R., Legouis, R., Lin, L., et al. (2015). Guidelines for monitoring autophagy in Caenorhabditis elegans. Autophagy *11*, 9–27.
36. Abdrakhmanov, A., Gogvadze, V., and Zhivotovsky, B. (2020). To eat or to die: deciphering selective forms of autophagy. Trends Biochem. Sci. *45*, 347–364.
37. Tian, Y., Li, Z., Hu, W., Ren, H., Tian, E., Zhao, Y., Lu, Q., Huang, X., Yang, P., Li, X., et al. (2010). C. elegans screen identifies autophagy genes specific to multicellular organisms. Cell *141*, 1042–1055.
38. Wu, F., Li, Y., Wang, F., Noda, N.N., and Zhang, H. (2012). Differential function of the two Atg4 homologues in the aggrephagy pathway in Caenorhabditis elegans. J. Biol. Chem. *287*, 29457–29467.
39. Kisurina-Evgenieva, O.P., Sutiagina, O.I., and Onishchenko, G.E. (2016). Biogenesis of micronuclei. Biochemistry (Mosc.) *81*, 453–464.
40. Triantaphyllou, A.C. (1983). Cytogenetic aspects of nematode evolution. In Concepts in Nematode Systematics, A.R. Stone, H.M. Platt, and L.F. Khalil, eds. (Academic Press).
41. Desjardins, C.A., Cerqueira, G.C., Goldberg, J.M., Dunning Hotopp, J.C., Haas, B.J., Zucker, J., Ribeiro, J.M., Saif, S., Levin, J.Z., Fan, L., et al. (2013). Genomics of Loa loa, a Wolbachia-free filarial parasite of humans. Nat. Genet. *45*, 495–500.
42. Ghedin, E., Wang, S., Spiro, D., Caler, E., Zhao, Q., Crabtree, J., Allen, J.E., Delcher, A.L., Guiliano, D.B., Miranda-Saavedra, D., et al. (2007). Draft genome of the filarial nematode parasite Brugia malayi. Science *317*, 1756–1760.
43. Hunt, V.L., Tsai, I.J., Coghlan, A., Reid, A.J., Holroyd, N., Foth, B.J., Tracey, A., Cotton, J.A., Stanley, E.J., Beasley, H., et al. (2016). The genomic basis of parasitism in the Strongyloides clade of nematodes. Nat. Genet. *48*, 299–307.
44. Kaessmann, H. (2010). Origins, evolution, and phenotypic impact of new genes. Genome Res. *20*, 1313–1326.
45. Ramm, S.A., Schärer, L., Ehmcke, J., and Wistuba, J. (2014). Sperm competition and the evolution of spermatogenesis. Mol. Hum. Reprod. *20*, 1169–1179.
46. Van Oss, S.B., and Carvunis, A.R. (2019). De novo gene birth. PLoS Genet. *15*, e1008160.
47. Luo, Z., Hu, T., Jiang, H., Wang, R., Xu, Q., Zhang, S., Cao, J., and Song, X. (2020). Rearrangement of macronucleus chromosomes correspond to TAD-like structures of micronucleus chromosomes in *Tetrahymena thermophila*. Genome Res. *30*, 406–414.
48. Huang, Y.J., Stoffel, R., Tobler, H., and Mueller, F. (1996). A newly formed telomere in Ascaris suum does not exert a telomere position effect on a nearby gene. Mol. Cell. Biol. *16*, 130–134.
49. Ottaviani, A., Gilson, E., and Magdinier, F. (2008). Telomeric position effect: from the yeast paradigm to human pathologies? Biochimie *90*, 93–107.
50. Loenen, W.A., Dryden, D.T., Raleigh, E.A., and Wilson, G.G. (2014). Type I restriction enzymes and their relatives. Nucleic Acids Res. *42*, 20–44.
51. Schatz, D.G., and Swanson, P.C. (2011). V(D)J recombination: mechanisms of initiation. Annu. Rev. Genet. *45*, 167–202.
52. Jung, D., Giallourakis, C., Mostoslavsky, R., and Alt, F.W. (2006). Mechanism and control of V(D)J recombination at the immunoglobulin heavy chain locus. Annu. Rev. Immunol. *24*, 541–570.
53. Bassing, C.H., Swat, W., and Alt, F.W. (2002). The mechanism and regulation of chromosomal V(D)J recombination. Cell *109* (*Suppl*), S45–S55.
54. Baudry, C., Malinsky, S., Restituito, M., Kapusta, A., Rosa, S., Meyer, E., and Bétermier, M. (2009). PiggyMac, a domesticated piggyBac transposase involved in programmed genome rearrangements in the ciliate Paramecium tetraurelia. Genes Dev. *23*, 2478–2483.
55. Bischerour, J., Bhullar, S., Denby Wilkes, C., Régnier, V., Mathy, N., Dubois, E., Singh, A., Swart, E., Arnaiz, O., Sperling, L., et al. (2018). Six domesticated PiggyBac transposases together carry out programmed DNA elimination in *Paramecium*. eLife *7*, e37927.
56. Cheng, C.Y., Vogt, A., Mochizuki, K., and Yao, M.C. (2010). A domesticated piggyBac transposase plays key roles in heterochromatin dynamics and DNA cleavage during programmed DNA deletion in Tetrahymena thermophila. Mol. Biol. Cell *21*, 1753–1762.
57. Cheng, C.Y., Young, J.M., Lin, C.G., Chao, J.L., Malik, H.S., and Yao, M.C. (2016). The piggyBac transposon-derived genes TPB1 and TPB6 mediate essential transposon-like excision during the developmental rearrangement of key genes in Tetrahymena thermophila. Genes Dev. *30*, 2724–2736.
58. Wang, Y., Wang, Y., Sheng, Y., Huang, J., Chen, X., Al-Rasheid, K.A.S., and Gao, S. (2017). A comparative study of genome organization and epigenetic mechanisms in model ciliates, with an emphasis on Tetrahymena, Paramecium and Oxytricha. Eur. J. Protistol. *61* (Pt B), 376–387.
59. Müller-Reichert, T., Hohenberg, H., O'Toole, E.T., and McDonald, K. (2003). Cryoimmobilization and three-dimensional visualization of C. elegans ultrastructure. J. Microsc. *212*, 71–80.
60. O'Toole, E.T., McDonald, K.L., Mäntler, J., McIntosh, J.R., Hyman, A.A., and Müller-Reichert, T. (2003). Morphologically distinct microtubule ends in the mitotic centrosome of Caenorhabditis elegans. J. Cell Biol. *163*, 451–456.
61. Redemann, S., Fürthauer, S., Shelley, M., and Müller-Reichert, T. (2019). Current approaches for the analysis of spindle organization. Curr. Opin. Struct. Biol. *58*, 269–277.

62. Hsu, J.Y., Sun, Z.W., Li, X., Reuben, M., Tatchell, K., Bishop, D.K., Grushcow, J.M., Brame, C.J., Caldwell, J.A., Hunt, D.F., et al. (2000). Mitotic phosphorylation of histone H3 is governed by Ipl1/aurora kinase and Glc7/PP1 phosphatase in budding yeast and nematodes. Cell *102*, 279–291.

63. de Castro, I.J., Gokhan, E., and Vagnarelli, P. (2016). Resetting a functional G1 nucleus after mitosis. Chromosoma *125*, 607–619.

64. Fuller, B.G., Lampson, M.A., Foley, E.A., Rosasco-Nitcher, S., Le, K.V., Tobelmann, P., Brautigan, D.L., Stukenberg, P.T., and Kapoor, T.M. (2008). Midzone activation of aurora B in anaphase produces an intracellular phosphorylation gradient. Nature *453*, 1132–1136.

65. Dedukh, D., Riumin, S., Chmielewska, M., Rozenblut-Kościsty, B., Kolenda, K., Kazmierczak, M., Dudzik, A., Ogielska, M., and Krasikova, A. (2020). Micronuclei in germ cells of hybrid frogs from Pelophylax esculentus complex contain gradually eliminated chromosomes. Sci. Rep. *10*, 8720.

66. Liu, M.L., and Yao, M.C. (2012). Role of ATG8 and autophagy in programmed nuclear degradation in Tetrahymena thermophila. Eukaryot. Cell *11*, 494–506.

67. Grishanin, A.K., and Zagoskin, M.V. (2018). Chromatin diminution in Cyclops kolensis Lill. (Copepoda, Crustacea) as a radical way to inactivate redundant genome in somatic cells. Cytogenet. Genome Res. *156*, 165–172.

68. Clower, M.K., Holub, A.S., Smith, R.T., and Wyngaard, G.A. (2016). Embryonic development and a quantitative model of programmed DNA elimination in Mesocyclops Edax (S. A. Forbes, 1891) (Copepoda: Cyclopoida). J. Crustac. Biol. *36*, 661–674.

69. Canela, A., Sridharan, S., Sciascia, N., Tubbs, A., Meltzer, P., Sleckman, B.P., and Nussenzweig, A. (2016). DNA breaks and end resection measured genome-wide by end sequencing. Mol. Cell *63*, 898–911.

70. Cheerambathur, D.K., Gassmann, R., Cook, B., Oegema, K., and Desai, A. (2013). Crosstalk between microtubule attachment complexes ensures accurate chromosome segregation. Science *342*, 1239–1242.

71. Desai, A., Rybina, S., Müller-Reichert, T., Shevchenko, A., Shevchenko, A., Hyman, A., and Oegema, K. (2003). KNL-1 directs assembly of the microtubule-binding interface of the kinetochore in C. elegans. Genes Dev. *17*, 2421–2435.

72. Dumont, J., Oegema, K., and Desai, A. (2010). A kinetochore-independent mechanism drives anaphase chromosome separation during acentrosomal meiosis. Nat. Cell Biol. *12*, 894–901.

73. Heath, C.M., and Wignall, S.M. (2019). Chromokinesin Kif4 promotes proper anaphase in mouse oocyte meiosis. Mol. Biol. Cell *30*, 1691–1704.

74. Karg, T., Elting, M.W., Vicars, H., Dumont, S., and Sullivan, W. (2017). The chromokinesin Klp3a and microtubules facilitate acentric chromosome segregation. J. Cell Biol. *216*, 1597–1608.

75. Karg, T., Warecki, B., and Sullivan, W. (2015). Aurora B-mediated localized delays in nuclear envelope formation facilitate inclusion of late-segregating chromosome fragments. Mol. Biol. Cell *26*, 2227–2241.

76. Redemann, S., Lantzsch, I., Lindow, N., Prohaska, S., Srayko, M., and Müller-Reichert, T. (2018). A switch in microtubule orientation during C. elegans meiosis. Curr. Biol. *28*, 2991–2997.e2.

77. Royou, A., Gagou, M.E., Karess, R., and Sullivan, W. (2010). BubR1- and Polo-coated DNA tethers facilitate poleward segregation of acentric chromatids. Cell *140*, 235–245.

78. Foster, J.M., Grote, A., Mattick, J., Tracey, A., Tsai, Y.C., Chung, M., Cotton, J.A., Clark, T.A., Geber, A., Holroyd, N., et al. (2020). Sex chromosome evolution in parasitic nematodes of humans. Nat. Commun. *11*, 1964.

79. Tandonnet, S., Koutsovoulos, G.D., Adams, S., Cloarec, D., Parihar, M., Blaxter, M.L., and Pires-daSilva, A. (2019). Chromosome-wide evolution and sex determination in the three-sexed nematode *Auanema rhodensis*. G3 (Bethesda) *9*, 1211–1230.

80. Hamilton, E.P., Kapusta, A., Huvos, P.E., Bidwell, S.L., Zafar, N., Tang, H., Hadjithomas, M., Krishnakumar, V., Badger, J.H., Caler, E.V., et al. (2016). Structure of the germline genome of *Tetrahymena thermophila* and relationship to the massively rearranged somatic genome. eLife *5*, e19090.

81. Chandra, T., Kirschner, K., Thuret, J.Y., Pope, B.D., Ryba, T., Newman, S., Ahmed, K., Samarajiwa, S.A., Salama, R., Carroll, T., et al. (2012). Independence of repressive histone marks and chromatin compaction during senescent heterochromatic layer formation. Mol. Cell *47*, 203–214.

82. Kimura, H., Hayashi-Takanaka, Y., Goto, Y., Takizawa, N., and Nozaki, N. (2008). The organization of histone H3 modifications as revealed by a panel of specific monoclonal antibodies. Cell Struct. Funct. *33*, 61–73.

83. Springhorn, A., and Hoppe, T. (2019). Western blot analysis of the autophagosomal membrane protein LGG-1/LC3 in Caenorhabditis elegans. Methods Enzymol. *619*, 319–336.

84. Ghurye, J., Rhie, A., Walenz, B.P., Schmitt, A., Selvaraj, S., Pop, M., Phillippy, A.M., and Koren, S. (2019). Integrating Hi-C links with assembly graphs for chromosome-scale assembly. PLoS Comput. Biol. *15*, e1007273.

85. Durand, N.C., Shamim, M.S., Machol, I., Rao, S.S., Huntley, M.H., Lander, E.S., and Aiden, E.L. (2016). Juicer provides a one-click system for analyzing loop-resolution Hi-C experiments. Cell Syst. *3*, 95–98.

86. Jain, C., Koren, S., Dilthey, A., Phillippy, A.M., and Aluru, S. (2018). A fast adaptive algorithm for computing whole-genome homology maps. Bioinformatics *34*, i748–i756.

87. Smit, A.F.A., Hubley, R., and Green, P. (2013). RepeatMasker Open 4.0. http://www.repeatmasker.org.

88. Ellinghaus, D., Kurtz, S., and Willhoeft, U. (2008). LTRharvest, an efficient and flexible software for de novo detection of LTR retrotransposons. BMC Bioinformatics *9*, 18.

89. Price, A.L., Jones, N.C., and Pevzner, P.A. (2005). De novo identification of repeat families in large genomes. Bioinformatics *21* (*Suppl 1*), i351–i358.

90. Novák, P., Neumann, P., Pech, J., Steinhaisl, J., and Macas, J. (2013). RepeatExplorer: a Galaxy-based web server for genome-wide characterization of eukaryotic repetitive elements from next-generation sequence reads. Bioinformatics *29*, 792–793.

91. Goubert, C., Modolo, L., Vieira, C., ValienteMoro, C., Mavingui, P., and Boulesteix, M. (2015). De novo assembly and annotation of the Asian tiger mosquito (Aedes albopictus) repeatome with dnaPipeTE from raw genomic reads and comparative analysis with the yellow fever mosquito (Aedes aegypti). Genome Biol. Evol. *7*, 1192–1205.

92. Li, W., and Godzik, A. (2006). Cd-hit: a fast program for clustering and comparing large sets of protein or nucleotide sequences. Bioinformatics *22*, 1658–1659.

93. Schindelin, J., Arganda-Carreras, I., Frise, E., Kaynig, V., Longair, M., Pietzsch, T., et al. (2012). Fiji: an open-source platform for biological-image analysis. Nat. Methods *9*, 676–682.

94. Mastronarde, D.N. (2005). Automated electron microscope tomography using robust prediction of specimen movements. J. Struct. Biol. *152*, 36–51.

95. Kremer, J.R., Mastronarde, D.N., and McIntosh, J.R. (1996). Computer visualization of three-dimensional image data using IMOD. J. Struct. Biol. *116*, 71–76.

96. Mastronarde, D.N. (1997). Dual-axis tomography: an approach with alignment methods that preserve resolution. J. Struct. Biol. *120*, 343–352.

97. Wang, J., Czech, B., Crunk, A., Wallace, A., Mitreva, M., Hannon, G.J., and Davis, R.E. (2011). Deep small RNA sequencing from the nematode

Ascaris reveals conservation, functional diversification, and novel developmental profiles. Genome Res. *21*, 1462–1477.

98. Wang, J., Garrey, J., and Davis, R.E. (2014). Transcription in pronuclei and one- to four-cell embryos drives early development in a nematode. Curr. Biol. *24*, 124–133.

99. Kang, Y., Wang, J., and Davis, R.E. (2017). Nuclei isolation from nematode *Ascaris*. Bio Protoc. *7*, e2262.

100. Belaghzal, H., Dekker, J., and Gibcus, J.H. (2017). Hi-C 2.0: An optimized Hi-C procedure for high-resolution genome-wide mapping of chromosome conformation. Methods *123*, 56–65.

101. Lieberman-Aiden, E., van Berkum, N.L., Williams, L., Imakaev, M., Ragoczy, T., Telling, A., Amit, I., Lajoie, B.R., Sabo, P.J., Dorschner, M.O., et al. (2009). Comprehensive mapping of long-range interactions reveals folding principles of the human genome. Science *326*, 289–293.

STAR★METHODS

KEY RESOURCES TABLE

REAGENT or RESOURCE	SOURCE	IDENTIFIER
Antibodies		
Mouse monoclonal anti-H3K36me2	Hiroshi Kimura [81]	Cat# 2C3; RRID: AB_2616102
Rabbit polyclonal anti-H3K4me1	Abcam	Cat# ab8895; RRID: AB_306847
Mouse monoclonal anti-H4K16ac	Hiroshi Kimura [81]	http://compbio.med.harvard.edu/antibodies/antibodies/258
Mouse monoclonal anti-H3K9me2	Hiroshi Kimura [81]	Cat# HK00008; RRID: AB_2616100
Mouse monoclonal anti-H3K9me3	Hiroshi Kimura [82]	Cat# HK00009; RRID: AB_2616099
Mouse monoclonal anti-H3K36me3	Hiroshi Kimura [82]	Cat# HK00012; RRID: AB_2616098
Mouse monoclonal anti-H3K27me3	Hiroshi Kimura [82]	Cat# 1E7; RRID: AB_2819243
Mouse monoclonal anti-H3K4me3 (clone CMA304)	Hiroshi Kimura/ Active Motif [81]	Cat# 61379; RRID: AB_2793611
Rabbit monoclonal anti-Lgg-1	[83]	N/A
Rabbit monoclonal anti-Ubiquitil H2A (K119) (clone D27C4)	Cell Signaling	Cat# 8240; RRID: AB_10891618
Rabbit polyclonal anti-H3S10P	Millipore	Cat# 06-570; RRID: AB_310177
Mouse monoclonal anti-Nuclear Pore Complex Proteins (clone Mab414)	Abcam	Cat# ab24609; RRID: AB_448181
Goat anti-Rabbit IgG (H+L) (AH) 15nm gold	Ted Pella	Cat# 15727
Biological Samples		
Ascaris suum	US Slaughterhouses	N/A
Chemicals, Peptides, and Recombinant Proteins		
CleanCut agarose, 2%	Bio-rad	Cat# 1703594
Proteinase K	Ambion	Cat# AM2548
Beta-agarase	NEB	Cat# M0392
Membrane Filter, 0.1 μm pore size	Millipore	Cat# VCWP04700
Glycoblue	Ambion	Cat# AM9515
LongAmp Taq DNA Polymerase	NEB	Cat# M0323
Nick Translation DNA Labeling System 2.0	Enzo	Cat# ENZ-GEN111
Gold 550 dUTP	Enzo	Cat# ENZ-42521
Red 650 dUTP	Enzo	Cat# ENZ-42522
SPRI beads	Beckman Coulter	Cat# B23318
Micro Bio-Spin P-30 Tris RNase-free	Bio-Rad	Cat# 7326251
Image-iT FX Signal Enhancer	Invitrogen	Cat# I36933
Prolong Diamond antifade mounting medium	Invitrogen	Cat# P36970
Deposited Data		
Raw sequence data	NCBI SRA	BioProject PRJNA62057
Genome assembly and annotation files	NCBI GenBank	JACCHR000000000
Oligonucleotides		
DNA FISH probe: Telomere: 5′-Quasar 570-TTAGGCTTAGGCTTAGGCTTAGGC	This paper	N/A
DNA FISH probe: 120 bp repeat: 5′-Fam-CGAATAAATCCCAATTGCAG	This paper	N/A
Primers for CBR DNA FISH probes, see Table S1	This paper	N/A
Software and Algorithms		
Canu v1.8	[27]	https://github.com/marbl/canu
SALSA	[84]	https://github.com/marbl/SALSA

(*Continued on next page*)

Continued

REAGENT or RESOURCE	SOURCE	IDENTIFIER
juicer v1.5.7	[85]	https://github.com/aidenlab/juicer
MashMap v2.0	[86]	https://github.com/marbl/MashMap
RepeatMasker v4.0.6	[87]	http://www.repeatmasker.org/
LTRharvest v1.5.6	[88]	https://www.zbh.uni-hamburg.de/
RepeatScout v1.0.5	[89]	https://bix.ucsd.edu/repeatscout/
RepeatExplorer v0.9.7.8	[90]	http://repeatexplorer.org
dnaPipeTE v1.2_04	[91]	http://lbbe.univ-lyon1.fr-dnaPipeTE-.html?lang=fr
CDhit v4.6.1	[92]	http://weizhongli-lab.org/cd-hit/
Fiji	[93]	https://fiji.sc/
SerialEM image acquisition software	[94]	https://bio3d.colorado.edu/SerialEM/
IMOD 4.9 tomography software package	[95, 96]	https://bio3d.colorado.edu/imod/
softWoRx	GE Healthcare and Applied Precision	N/A
Oligo 7	Oligo Primer Analysis Software	Cat# M7SF02

RESOURCE AVAILABILITY

Lead Contact

Further information and requests for resources and reagents should be directed to and will be fulfilled by the Lead Contact Richard E. Davis (richard.davis@cuanschutz.edu) or Jianbin Wang (jianbin.wang@utk.edu).

Materials Availability

Materials from this study are available on request.

Data and Code Availability

DNA sequences and genome assemblies are deposited at the NCBI SRA in BioProject PRJNA62057 and at NCBI GenBank: JACCHR000000000.

EXPERIMENTAL MODEL AND SUBJECT DETAILS

All *Ascaris suum* material are derived from wild adult and females collected at US Slaughterhouses from the intestines of pigs.

METHOD DETAILS

Ascaris and megabase-size DNA isolation

Collection of pig *Ascaris suum* tissues, zygotes, and embryonation were as previously described [97, 98]. DNA isolation for PacBio sequencing was prepared from embryos embedded in agarose. The chitinous shell was removed by treatment for 90 min in 0.5 N NaOH and sodium hypochlorite at 30°C followed by extensive washing in PBS, pH 7.4. The embryos were treated for 1 min in 90% isopropanol (this removes the ascaroside-based impermeable layer), washed with PBS, pH 7.4, suspended in 10 mM Tris, pH 7.2, 20 mM NaCl, 50 mM EDTA and embedded in 2% CleanCut agarose (BioRad) in BioRad plug molds for a final agarose concentration of 0.75%. Agarose plugs were incubated in 2.5 mL of lysis buffer (10 mM Tris pH 8, 25 mM EDTA, 100 mM NaCl, 0.5% SDS) with 1.4 mg/mL Proteinase K (Ambion, AM2548) in a 50°C water bath for 2 h with intermittent mixing and then overnight with fresh Proteinase K solution. The plugs were extensively rinsed and washed (3X rinse and 5X wash) in 10 mM Tris pH 8.0, 50 mM EDTA and then rinsed and washed twice in 10 mM Tris pH 8.0, 1mM EDTA. To release and extract the genomic DNA, the plugs were digested with beta-agarase (NEB M0392) as described by the manufacturer to liberate DNA, followed by drop-dialysis (VCWP04700 Millipore) against 15 mL of TE buffer. The DNA was further treated with 0.1% SDS and proteinase K (400 ug/mL) before precipitation with 15 μg of glycoblue carrier (Ambion, AM9515), 0.3 M NaOAc pH 5.2, and 2.5 volumes of 100% ethanol. The precipitated DNA was dissolved in low TE buffer (10 mM Tris-HCl pH 8.0, 0.1 mM EDTA) or water.

PacBio sequencing and initial assembly

Two PacBio libraries derived from 2-cell (48 h) and 4-cell (65 h) embryo DNA were prepared and sequenced by the University of Washington PacBio Sequencing Services (https://pacbio.gs.washington.edu/) using the Sequel II system. From two SMRT Cell

runs, we obtained ~360X raw reads with average read length of 15 kb. PacBio reads over 40 kb (average 52 kb, total ~100X read coverage) were used to assemble the initial germline genome assembly using Canu [27] with parameters "corOutCoverage=1000 correctedErrorRate=0.105 corMinCoverage=0 genomeSize=330m." The initial assembly had 763 contigs with N50 = 4.83 Mb (N50 number = 23).

Hi-C data and scaffolding

Nuclei isolated as described [26, 99] from both germline (testis) and somatic cells (5-day, 32-64 cell embryos) were used to generate Hi-C libraries using an adapted protocol [100, 101]. The Hi-C data were used to further scaffold the initial contigs into chromosomes. Briefly, we first scaffolded the 763 contigs into 570 scaffolding (N50 = 10.24 Mb; N50 number = 13) using SALSA [84]. We then divided these scaffolds into 24 groups that correspond to the 24 germline chromosomes based on the contact information using Juicer and Juicebox [85]. For each chromosome group, we then mapped all original PacBio reads (360X) using MashMap [86] to retrieve all reads that can be uniquely mapped to the chromosome. The PacBio reads for each chromosome were then independently assembled using Canu, resulting in only 1 or 2 dominant contigs per chromosome for 20 chromosomes (the other 4 chromosomes have 3 or 4 large contigs). Each chromosome assembly was further evaluated manually using Juicer and Juicebox and scaffolded when necessary. The final assembly contains 24 scaffolds (N50 = 12.43 Mb; N50 number = 9) and 84 unplaced small contigs (2.3% of the genome).

Genes and their tissue-specific expression analysis

We mapped our previously defined transcripts [14] to define genes in the new genome assembly. Over 99.9% (61,766/61,820) of the genome-based transcripts and over 95.7% (59,965/62,645) *de novo* assembled transcripts can be mapped to the new genome, suggesting the current genome assembly is highly complete. To gauge the tissue-specific expression of the genes, we used RNA-seq data from 9 broadly defined tissues from *Ascaris*, including testis, ovary, zygote (zygote1-4), early embryos (1-4 cell, 24 h-64 h), late embryos (16 - >500 cell, 96 h - 7day), larvae (L1 - L3), carcass, muscle and intestine [14, 20, 98]. The tissue-specific expression was scored by comparing each gene's RNA level (rpkm) in the tissue where this gene is mostly highly expressed (has the highest rpkm) to the other 8 tissues. The expression of the gene in the tissue is considered as tissue specific (score = 100) if its expression is 4-fold higher than in any of the other 8 tissues. The fewer the number of tissues that meet the 4x expression cutoff the less tissue-specific the expression of the gene. Genes with expression < 4X higher than in all other tissues are considered as genes without tissue specific expression (score = 0); these genes are most likely house-keeping genes, particularly if their overall expression level is high.

Repetitive sequence identification

Repetitive sequences were identified using a combination of homology-based and *de novo* approaches, including RepeatMasker [87], LTRharvest [88], RepeatScout [89], RepeatExplorer [90], and dnaPipeTE [91]. The repeats library was filtered for redundancy with CD-hit [92].

Antibodies and immunohistochemistry

Monoclonal histone antibodies used (H3K9me2, H3K9me3, H3K36me2, H3K36me3, H3K27me3, H3K4me3, and H4K16ac) were from Hiroshi Kimura [81, 82] and have been previously validated for use in the modENCODE project for *C. elegans* and other organisms (see antibody validation database: http://compbio.med.harvard.edu/antibodies/). The *C. elegans* Lgg-1 antibody was provided by Thorsten Hoppe [83] and detects both the non-lipidated (LGG-1-I) and the lipidated (LGG-1-II) forms of LGG-1. Commercial antibodies were obtained for rabbit Ubiquityl-Histone H2A (Lys119) (Cell Signaling D27C4), rabbit H3S10P (Millipore 06-570), rabbit H3K4me1 (Abcam ab8895), and Nuclear Pore Complex Proteins (Abcam Mab414). *Ascaris* embryo immunohistochemistry was carried as described [26, 98] using a modified freeze-crack method to permeabilize and fix embryos with some modifications. Briefly, decoated embryos were suspended in 50% methanol and 2% formaldehyde solution and were frozen and thawed 3 times using a dry ice/ethanol bath. The embryos were re-hydrated with 25% methanol in PBS pH 7.4 for 1 min. After washing twice with PBS pH 7.4, the embryos were suspended in blocking solution (0.5% BSA in PBS pH 7.4) for 1 h at room temperature, followed by overnight incubation in primary antibodies at 4°C, and then a 2 h incubation in secondary antibodies (Invitrogen) at room temperature. Nuclei were stained with DAPI and slides mounted in anti-fade medium (Invitrogen).

DNA FISH Probes

Telomere (5′-Quasar 570-TTAGGCTTAGGCTTAGGCTTAGGC) and 120 bp repeat (5′-Fam-CGAATAAATCCCAATTGCAG) oligonucleotide probes were obtained from LGC Biosearch (Petaluma, CA). For unique sequence FISH, 5-11 kb PCR products covering a total of 12-32 kb were generated for both retained and eliminated genome regions adjacent to internal and subtelomeric chromosome breaks. PCR primers were designed using the Oligo 7 software and PCR was performed using Long-Amp Taq DNA polymerase (New England Biolabs) following the manufactures directions. PCR products for a region were pooled, purified with SPRI beads (Beckman Coulter) and labeled with Gold 550 dUTP (Enzo) or Red 650 dUTP (Enzo) by nick translation using the Nick Translation DNA Labeling System 2.0 kit (Enzo). Labeled probes were then purified using Micro Bio-Spin Columns with Bio-Gel P-30 (BioRad).

DNA FISH

A freeze-crack method was used to permeabilize [26, 98] and fix the embryos in methanol/acetic acid (3:1). Methanol/acetic acid-fixed embryos were progressively rehydrated with 90%, 70%, 50% and 25% MeOH in PBS pH 7.4 for 10 min each at room

temperature. Embryos were then washed once with PBS pH 7.4 and treated with 100 ug/mL RNase A in PBS pH 7.4 for 30 min at 37°C, followed by incubation in signal enhancer solution (Invitrogen) for 30 min at room temperature. Next, embryos were re-suspended in blocking solution (1% BSA in PBS pH 7.4) for 1 h at room temperature and re-fixed in fresh 3.7% paraformaldehyde/1X PBS for 10 min at room temperature. Embryos were then washed with PBS pH 7.0, 2X SSC, and then incubated for 2 h at 37°C in pre-hybridization buffer (10% formamide in 2X SSC). Following pre-prehybridization, embryos were denatured in denaturation buffer (oligonucleotide probe buffer = 50% formamide in 2X SSC; Nick-translated probe buffer = 70% formamide in 2X SSC) for 5 min at 75°C. Oligonucleotide hybridization was carried out with 400 nM probes (telomere and 120 bp repeat) in hybridization buffer 1 (10% formamide/10% dextran sulfate/0.5 μg/μL salmon sperm DNA/0.2% SDS/2X SSC) overnight at 37°C. Duplex DNA probes were denatured for 5 min at 75°C, placed on ice for 2 min, pre-warmed at 37°C, and hybridization was carried out with 50 ng of nick-translated probe in hybridization buffer 2 (50% formamide/10% dextran sulfate/0.5 μg/μL salmon sperm DNA/0.2% SDS/2X SSC) overnight at 37°C. Post-hybridization washes for oligonucleotide probes were done in 2X SSC/0.1% Nonidet-P40 at 37°C for 5 min and for unique probes in 0.4X SSC at 45°C for 15 min followed by 2X SSC/0.1% Nonidet-P40 at room temperature for 10 min. Nuclei were stained with DAPI, slides mounted in anti-fade medium (Invitrogen), and kept in the dark at room temperature for 24 h before imaging.

Image acquisition

Ascaris embryo immunohistochemistry and FISH images were acquired on an Applied Precision DeltaVision microscope, using a 60X immersion objective and FITC/Cy3/Cy5/DAPI excitation filter sets. Images were deconvolved with Applied Precision's Softworx software and analyzed using Fiji software [93].

Preparation of *Ascaris* embryos for electron microscopy

Embryos were prepared for electron microscopy using high pressure freezing and freeze substitution essentially as described [59] with the following modifications. Intact 4 cell and 8-16 cell embryos were collected as described above, mixed with 15% dextran, loaded into 100 μm or 200 μm aluminum planchettes, and then rapidly frozen under high pressure in a Wohlwend Compact 02 High Pressure Freezer (Technotrade International). The frozen samples were then freeze substituted in 2% OsO4 and 0.2% uranyl acetate in acetone for three days at −80°C, rinsed in acetone, warmed to −20°C, 4°C and then room temperature and embedded in Epon resin over 4 days. For immunolabeling, the frozen samples were freeze substituted in 0.1% glutaraldehyde and 0.01% uranyl acetate in acetone and embedded in Lowicryl HM20.

Serial section electron microscopy, immuno-EM and electron tomography

Serial, 100-200 nm thick sections were cut using a Leica Ultracut UCT microtome. Sections were collected onto formvar-coated, copper slot grids and post stained with 2% uranyl acetate and Reynolds lead citrate. The grids with serial sections were imaged using a Tecnai T12 microscope to identify embryos with mitotic cells, track the spindle through serial sections and to confirm the cell stage of a particular embryo.

For immuno-electron microscopy, serial, thin (80nm) sections were collected onto formvar-coated nickel slot grids. The grids were incubated in a blocking buffer containing 0.1% or 0.2% nonfat dry milk dissolved in PBS/Tween20, followed by incubation with the H3S10P antibody at 1:10 or 1:50 dilution. Control grids were incubated in blocking buffer without the primary antibody. The grids were rinsed and incubated with a rabbit secondary antibody conjugated to 15 nm gold at a 1:20 dilution in blocking buffer (Ted Pella, Redding, CA). Grids were post stained with 2% uranyl acetate and Reynolds lead citrate and imaged in a Tecnai T12 microscope. Images from serial sections were collected to confirm labeling on specific organelles.

Tomography was performed as essentially as described [60]. Briefly, grids containing serial, 200nm thick sections were imaged using a Tecnai F30 (Thermo Fisher Scientific, Waltham, MA) operating at 300kV. Montaged images were collected using a Gatan OneView camera (Gatan, Pleasanton, CA) to record images at a 1.7nm pixel size over an area approximately 7μm x 7μm. Single axis tilt series were collected over a +60° to −60° range at 1° increments using the SerialEM image acquisition program [94]. The tilted views were aligned using local patch tracking and tomograms generated using the IMOD 4.9 software package (https://bio3d.colorado.edu/imod/) [95, 96].

Tomograms were displayed and microtubules modeled using the 3dmod program of the IMOD software package. The image slicer window was used to orient a slice of image data to follow and track individual MTs along their lengths. The model contours were projected in 3D and rotated to study the spindle MT organization during DNA elimination mitosis.